Dalton Transactions

Recent advances in cooperative activation of CO2 and N2O by bimetallic coordination complexes or binuclear reaction pathways

SCHOLARONE™
Manuscripts

ARTICLE

Recent advances in cooperative activation of CO_2 and N_2O by bimetallic coordination complexes or binuclear reaction pathways

Soumen Sinhababu[a], Yutthana Lakliang[a], and Neal P. Mankad[a,*]

The gaseous small molecules, CO_2 and N_2O, play important roles in climate change and ozone layer depletion, and they hold promise as underutilized reagents and chemical feedstocks. However, productive transformations of these heteroallenes are difficult to achieve because of their inertness. In nature, these gases are cycled through ecological systems by metalloenzymes featuring mutlimetallic active sites that employ cooperative mechanisms. Thus, cooperative bimetallic chemistry is an important strategy for synthetic systems, as well. In this Perspective, recent advances (since 2010) in cooperative activation of CO_2 and N_2O are reviewed, including examples involving *s*-block, *p*-block, *d*-block, and *f*-block metals and different combinations thereof.

Introduction

Carbon dioxide (CO_2) and nitrous oxide (N_2O) are two of the three most prominent anthropogenic greenhouse gases, with CO_2 having ~12x higher atmospheric abundance and N_2O having ~300x higher global warming potential.[1] Anthropogenic N_2O emissions are also a leading cause of ozone layer depletion.[2] Thus, it is important to gain fundamental understanding of how these gaseous small molecules can be efficiently captured and transformed. Notably, both molecules also hold great promise as synthetic reagents. The use of CO_2 as a C1 feedstock is an active area of research,[3,4] in part due to the dramatically lower toxicity and flammability of CO_2 compared to more commonly used CO. Similarly, N_2O can be viewed as a green oxidant, producing benign N_2 as its only byproduct.[5] Considering the activation of these gases together is also sensible because, as heteroallenes, CO_2 and N_2O are isoelectronic and isolobal to each other.

Several challenges need to be overcome in this area. First, both CO_2 and N_2O are relatively inert towards binding to many transition metal active sites. For example, Taube measured that displacement of N_2O from $[Ru(NH_3)_5(N_2O)]^{2+}$ by N_2 to form $[Ru(NH_3)(N_2)]^{2+}$ is actually favorable thermodynamically and facile kinetically.[6] Second, transformations of CO_2 and N_2O to useful products often require catalytic architectures capable of multielectron redox cycling. For example, conversion of CO_2 to CH_3OH is a 4-electron redox reaction, and hypothetical oxidation of substrates by N_2O are 2-electron redox reactions. Thus, especially for non-precious metal systems, multinuclear assemblies are particularly promising since these metals often favor 1-electron redox chemistry. Indeed, natural systems responsible for ecological carbon/nitrogen cycling employ multinuclear metalloenzyme active sites to transform these substrates. While building biomimetic clusters that are both structurally faithful to the natural systems and replicate their catalytic efficiency has been challenging,[7] the cooperative behavior is more readily mimicked in structurally dissimilar systems that employ multimetallic active sites or binuclear reaction pathways for small molecule activation.

In the case of CO_2, bacterial and archaeal carbon monoxide dehydrogenase (CODH) enzymes catalyze two-electron redox interconversions of CO and CO_2. Aerobic and anaerobic variants feature Mo/Cu and Ni/Fe active sites, respectively.[8,9] In both cases, activated μ_2-1,2-CO_2 intermediates are thought to involve cooperative binding between two metal sites, one of which is Lewis acidic and the other of which is Lewis basic (Figure 1a). This bifunctional behavior was first mimicked synthetically by Floriani in 1978,[10] using an anionic Co(I) salen in which a K^+ counter cation was at an appropriate distance to stabilize a bimetallic [Co-C(=O)-O-K] unit (Figure 1b). Since that time, multiple related heterobimetallic CO_2 adducts have been characterized.[11–14] More recently, such cooperative behavior has even been observed in metal-free frustrated Lewis pairs (FLPs, Figure 1c).[15]

[a.] Department of Chemistry, University of Illinois at Chicago, 845 W. Taylor St., Chicago, IL 60607, USA
* npm@uic.edu
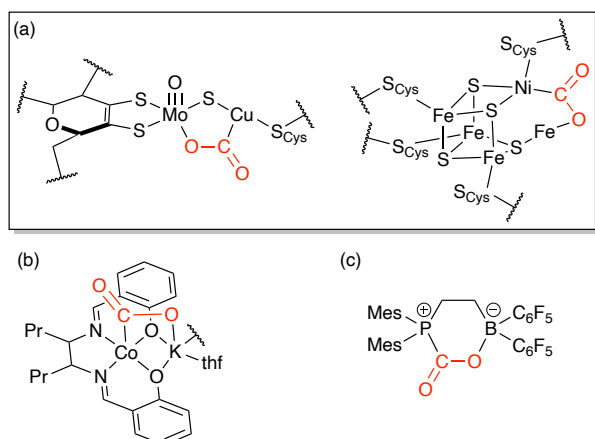
Figure 1. Cooperative CO_2 binding by Lewis acid/base pairs: (a) aerobic and anaerobic CODH active sites, (b) Co(I) salen with K^+ counter cation, (c) intramolecular FLP.

Similarly, during bacterial denitrification, N_2O is converted to N_2 and H_2O by nitrous oxide reductase (N_2OR), featuring the tetranuclear Cu_Z active site responsible for N_2O binding. Here, too, it is thought that cooperative activation of N_2O occurs along an edge of the Cu_Z cluster featuring two Cu centers with inhomogeneous electron density distribution (Figure 2a),[16] although the computationally modeled μ_2-1,3-N_2O adduct has never been observed experimentally. In the earliest success at biomimicry, the Tolman group demonstrated that N_2O reduction by a fluxional multicopper assembly proceeds through a critical, binuclear transition state with μ-1,1,-O binding (Figure 2b).[17] As with CO_2, FLPs are known to bind N_2O effectively.[18] Strong parallels exist between these precedents and the heterogeneous catalyst, Cu-ZSM-5, known to mediate oxidation of methane to methanol using N_2O as an O-atom source. The Sels, Schoonheydt. and Solomon groups conducted combined experimental/computational studies of this system,[19,20] ultimately demonstrating that N_2O activation occurs at localized dicopper(I) pairs with ~4.2-Å spacing enforced by the zeolite support. Following N_2O binding by a μ-1,1-O coordination mode (Figure 2c), supported $[Cu_2O]^{2+}$ sites are produced as reactive O-atom transfer intermediates.
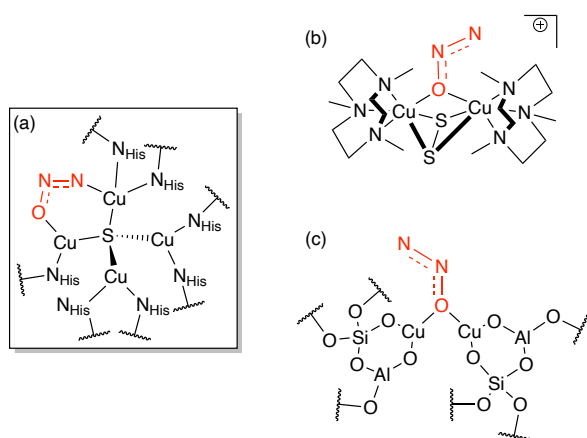
In this Perspective, we review recent advances in cooperative activation of CO_2 and N_2O, either by binuclear metal complexes or by mononuclear metal complexes operating by binuclear mechanisms. Only reports since 2010 are included, corresponding to a timeframe in which cooperative small molecule activation has seen resurgence in the transition metal literature. Cooperative behavior of homobinuclear metalloid complexes and heterobinuclear metal/metalloid complexes are not discussed in detail despite recent important advances.[21,22] Only examples of thermal chemistry are included, thus excluding exciting recent advances in the areas of electro- and photochemistry.[23–27]

Bimetallic CO_2 activation

Early transition metal bimetallic complexes

In 2014, Cloke and co-workers reported the synthesis and characterization of a bimetallic titanium complex, $(\mu:\eta^5,\eta^5\text{-}Pn^\dagger)_2Ti_2$ (**1a**) ($Pn^\dagger = [C_8H_4\{Si^iPr_3\text{-}1,4\}_2]^{2-}$) with a very short Ti=Ti bond.[28] Complex **1a** reductively splits CO_2 to form a bis(oxo) bridged dimer $[(\eta^8\text{-}Pn^\dagger)Ti(\mu\text{-}O)]_2$ (**1b**), in which the Ti=Ti bond has been cleaved, and the dicarbonyl complex $(\mu:\eta^5,\eta^5\text{-}Pn^\dagger)_2[Ti(CO)]_2$ (**1c**) in 1:1 ratio (Scheme 1). A mechanistic investigation was reported in 2015, in which key intermediates were identified using spectroscopic and computational techniques.[29] The reaction of **1a** with 1 equiv of CO_2 (or $^{13}CO_2$) was carried out in methylcyclohexane-d_{14} (MeCy-d_{14}) at -78 °C (Scheme 1). A color change from deep red to dark green was observed, due to quantitative conversion of **1a** to an intermediate species, **1d**, that was detected by low-temperature spectroscopic measurements (at -30 °C). Characteristic OCO vibrational frequencies of **1d** showed a shift from 1678 and 1236 cm^{-1} to 1637 and 1217 cm^{-1}, respectively, upon ^{13}C isotopic labelling, allowing the authors to assign a bent OCO structure fo **1d** in agreement with computational predictions. Upon warming **1d** to ambient temperature under dynamic vacuum, the red mono(oxo) complex **1e** was isolated. At room temperature, a C_6D_6 solution of **1e** slowly converted to green crystals of **1f**. A reaction energy diagram for the transformation was provided by computational modeling.
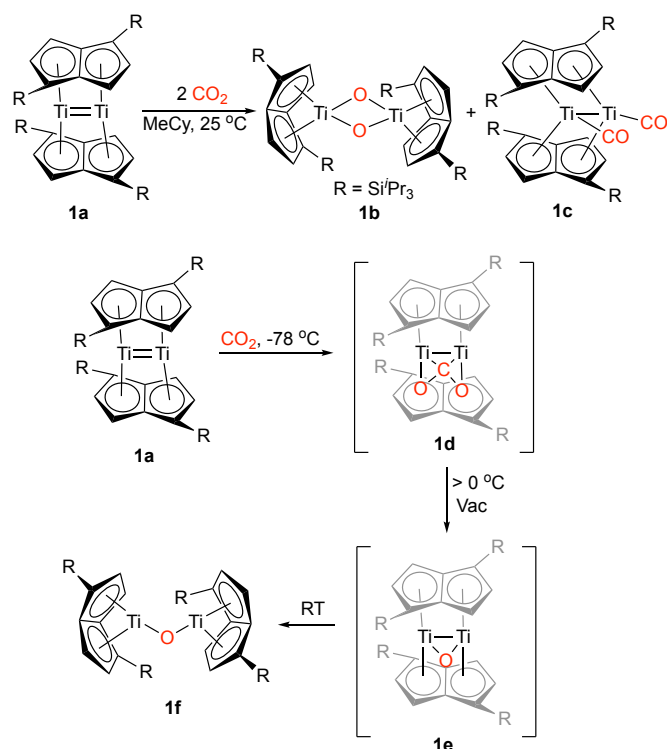

Figure 2. Cooperative N_2O binding by Cu-containing active sites: (a) the Cu_Z site of N_2OR, (b) a synthetic model complex, and (c) the Cu-doped zeolite material, Cu-ZSM-5.

Scheme 1. Stepwise reactions of CO_2 with Ti=Ti complex

CO$_2$ activation by a chromium-chromium quintuple bond was reported by Kempe group. The reaction of CO_2 with chromium dimer **2a** leads to C=O bond cleavage to give a CO bridged diamagnetic complex **2b** (Scheme 2) in 26% isolated yield. The solid state IR spectrum of complex **2b** shows strong absorption bands at 1924 and 1806 cm^{-1} due to carbonyl ligands.[30] NMR experiments were carried out to examine the by-product resulting from the oxygen released. NMR spectra showed **2b** is the major product along with some broad peaks due to a paramagnetic compound, although the structural identity was unknown, and no further mechanistic study were carried out.
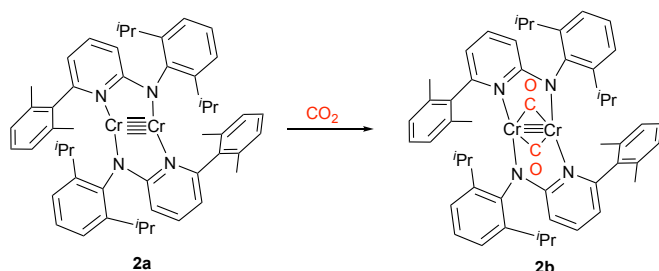
**Scheme 2.** Activation of CO_2 by a Cr$_2$ quintuply-bonded complex

Cummins, Okuda, and Maron groups isolated the first dimetalloxycarbene complex **3a**, prepared through multistep synthetic route starting from TiX$_3$ (X = N-[^{t}Bu](3,5-Me$_2$C$_6$H$_3$)). **3a** was found to be stabilized by fluxional coordination of the carbenic carbon atom to both metal centers.[31] This complex **3a** reacts cleanly with CO_2 to generate the bridging oxalate complex [(TiX$_3$)$_2$(μ_2-C$_2$O$_4$-κO:κO″)] (**3b**) (Scheme 3). The crystal structure of **3b** is centrosymmetric with an oxalato ligand

bridging two titanium atoms in a κ^1:κ^1 fashion. Theoretical calculations revealed rearrangement of the unsymmetrical bridging carbondioxo ligand to an intriguing μ-κ^1:κ^1 dimetalloxycarbene isomer (**3a**) which enables the aforementioned reduction of CO_2 to give oxalate.
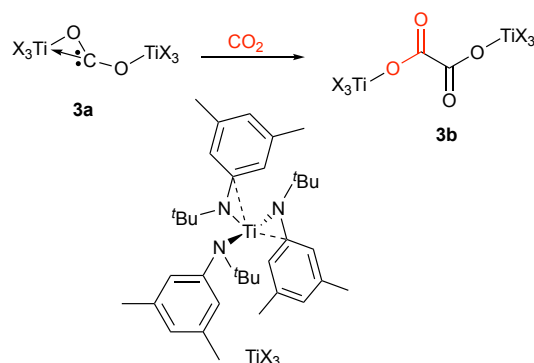
**Scheme 3.** Activation of CO_2 by bimetallic Ti system

Early/late transition metal bimetallic complexes

As opposed to homobimetallic systems, heterobimetallic systems have polar metal-metal bonds that are well suited to activate the polar C=O bond of CO_2. This effect is particularly strong for early/late heterobimetallic complexes. Since the seminal report of bifunctional CO_2 activation by Floriani in 1978,[10] several examples of early/late heterobimetallic activation of CO_2 were reported prior to 2000.[12–14] In all those cases CO_2 coordination occurs but C-O bond cleavage does not. The first C-O bond cleavage by an early/late heterobimetallic complex was reported by Thomas group.[32] Reaction of **4a** with CO_2 in THF at low temperature leads to formation of (OC)Co(^{i}Pr$_2$PNMes)$_2$-(μ-O)Zr(^{i}Pr$_2$PNMes) (**4b**), where one of the C=O double bonds of CO_2 has oxidatively added across the Zr-Co multiple bond in **4a** (Scheme 4).[32] **4b** is a paramagnetic complex with a characteristic IR feature at 1926 cm^{-1} for the carbonyl group. The authors hypothesized that hemilability of the phosphinoamide ligand is the crucial to this reactivity, as migration of one phosphine ligand from Co to Zr provides substrate access to the metal-metal bond.
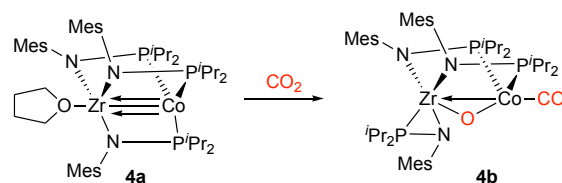
Scheme 4. Activation of CO_2 by heterobimetallic Zr/Co complex

Later Thomas and co-workers reported reactivity of [(L)M][OZr(MesNP^{i}Pr$_2$)$_3$Co(CO)] (M = Li, L = 12-c-4, **5a**; M = K, L = 18-c-6, **5b**), derived from **4b**, toward 1 equiv of CO_2.[33] ^{1}H NMR spectroscopy revealed shifts in the paramagnetic peaks of the phosphinoamide ligand, and the structure was later assigned to be [L(M)][(μ-κ^1,κ^2-CO$_3$)]Zr(MesNP^{i}Pr$_2$)$_3$Co(CO)] (M = Li, L = 12-c-4, **5c**; M = K, L = 18-c-6, **5d**) (Scheme 5). These Zr-carbonate

complexes (**5c** and **5d**) were further found to incorporate isotopically labelled ^{13}C upon exposure to $^{13}CO_2$ gas.
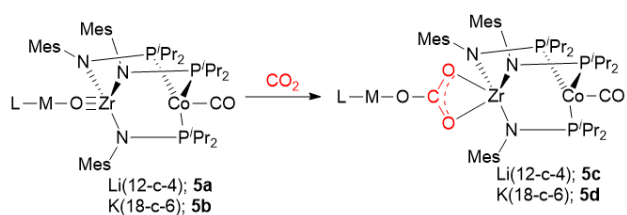
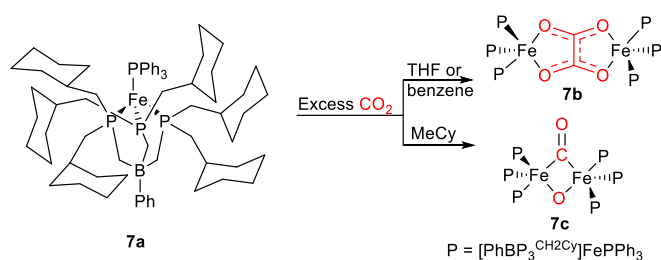**Scheme 5.** Reaction of CO_2 with a low-valent heterobimetallic Zr/Co complex

Late transition metal bimetallic complexes

Bownman and co-workers described a dinuclear copper(I) complex (**6a**) oxidized in air by CO_2 rather than O_2.[34] The yellow-colored solution of dinuclear copper(I) complex turned greenish-blue upon exposure to air and tetranuclear copper(II) complex (**6b**) was isolated in 72% yield (Scheme 6). X-ray crystallography revealed the presence of bridging oxalate anions derived from CO_2 in the air. Further treatment of the tetranuclear copper(II) oxalate complex (**6b**) in acetonitrile with $LiClO_4$ (a soluble lithium salt) resulted in quantitative precipitation of lithium oxalate. Moreover, the authors found that dicopper(I) complex could be used as an electrocatalyst for the reductive coupling of CO_2 to oxalate.
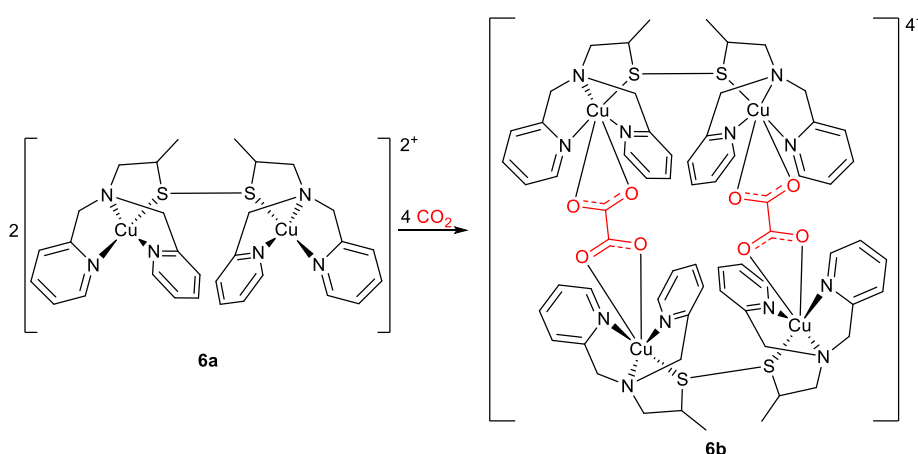

Scheme 6. Reductive coupling of CO_2 to oxalate by a dicopper(I) complex.

Peters and co-workers revealed an interesting and unexpected role for the solvent medium in CO_2 activation reaction using reactive iron(I) complexes supported by tris(phosphino)borate ligands, $[PhBP_3^R]^-$ ($[PhBP_3^R]^-$ = $[PhB(CH_2PR_2)_3]^-$; R = CH_2Cy, Ph, ^iPr, $m$ter; $m$ter = 3,5-*meta*-terphenyl).[35] Exposure of a benzene solution of PPh_3-adduct **7a** to 1 atm CO_2 resulted in a color change from dark orange to dark red, and both NMR and IR analysis showed a clean, though incomplete, conversion to the bridging oxalate product **7b** over a period of 26 h (Scheme 7). In THF solvent, a similar selectivity was observed, although after 26 h only 30% conversion to **7b** was observed. In contrast, when the reaction between **7a** and CO_2 was carried out in MeCy, C=O cleavage product **7c** was produced in low yield (10%) (Scheme 7). Similar results were obtained with PCy_3-adduct $[PhBP_3^{CH2Cy}]FePCy_3$.

Next the authors examined the role of the $[PhBP_3^R]^-$ ligand systems in the reaction between iron(I) and CO_2 by *in-situ* reducing of $[PhBP_3^R]FeCl$ derivatives with Na/Hg in the presence of CO_2 (R = ^iPr, MeCy). When $[PhBP_3^{CH2Cy}]FeCl$ (**8a**) was used as the Fe source, μ-oxalate **7b** was isolated as the major species (50%) with no observation of **7c** (Scheme 8).[35] In contrast, the reduction of $[PhBP_3^{iPr}]FeCl$ (**8b**) under CO_2 atmosphere leads to C=O cleavage selectively, and identified products were $\{[PhBP_3^{iPr}]Fe\}_2(μ\text{-}O)$ (**8c**) and $[PhBP_3^{iPr}]Fe(CO)_2$ (**8d**) (Scheme 8). The *in situ* reduction of $[PhBP_3^{Ph}]FeCl$ (**8e**) under an atmosphere of CO_2 resulted again C=O cleavage, generating $\{[PhBP_3^{Ph}]Fe\}_2(μ\text{-}O)$ (**8f**), $[PhBP_3^{Ph}]Fe(CO)_2$ (**8g**), and$\{[PhBP_3^{Ph}]Fe(CO)_2\}\{Na(THF)_5\}$ (**8h**) (Scheme 8). Reduction of more bulky $[PhBP_3^{mter}]FeCl$ under CO_2 atmosphere afforded no reaction. From these outcomes they suggested relative steric profiles dominates the CO_2 reduction product selectivity.[35] Although no intermediates were detected directly, from the collected observations it is assumed that a binuclear pathway is involved in oxalate formation, whereas decarbonylation may proceed by a mononuclear rate-determining step.


Scheme 7. Solvent-dependent reactivity of CO_2 with an Fe(I) complex
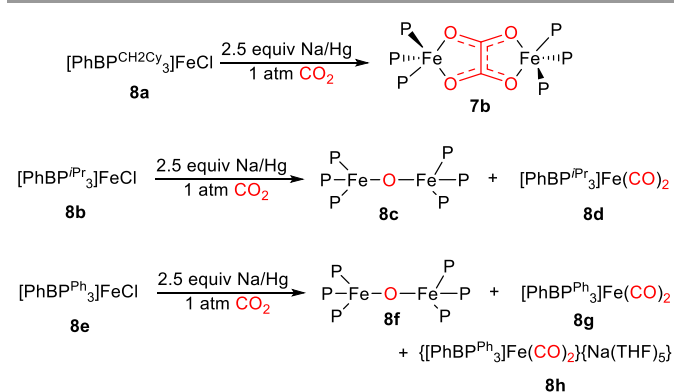
Scheme 8. Reaction of CO_2 with *in-situ* generated Fe(I) complexes

Suzuki and co-workers reported photochemical reaction of diruthenium tetrahydride-bridged complexes with CO_2.[36] Depending on cyclopentadienyl ligand systems two types of products, (i) a μ-formato complex and (ii) a μ-carbonyl-μ-oxo, complex were formed. UV irradiation of $Cp^*Ru(\mu$-H$)_4RuCp^*$ (**9a**) in THF under atmospheric CO_2 at 0 °C for 24 h afforded a bridging-formato complex, $Cp^*Ru(\mu$-OCHO$)(\mu$-H$)_3RuCp^*$ (**9b**) (Scheme 9). In contrast, sterically demanding 1,2,4-tri-*tert*-butylcyclopentadienyl-ligated complex, $Cp^{\ddagger}Ru(\mu$-H$)_4RuCp^{\ddagger}$ (**9c**), reacted with 1 atm of CO_2 under UV condition in benzene at ambient temperature to form a μ-carbonyl-μ-oxo complex, $Cp^{\ddagger}Ru(\mu$-CO$)(\mu$-O$)RuCp^{\ddagger}$ (**9d**), via cleavage of a C=O double bond (Scheme 9).[36] It was worth mentioning that thermal reactivity of these complexes with CO_2 was not observed irrespective of substituents on the Cp ring of the auxiliary ligands.
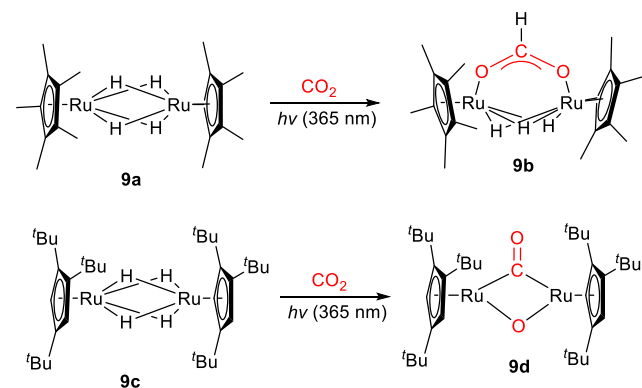
Scheme 9. Photochemical activation of CO_2 by hydride-bridged diruthenium complexes

Ozerov group reported reaction of CO_2 with a Pd(I)-Pd(I) dimer stabilized by bis(phosphino)amide pincer PNP ligands in the presence of Me_3SiCl and Me_3SiOTf, producing free CO.[37] Initial reaction of C_6D_6 solution of **10a** with 1 atm of CO_2 at ambient temperature or at 80 °C, or under UV light, did not produce any NMR-detectable products (Scheme 10). In contrast, reaction of **10a** with CS_2, a heavier analog of CO_2, resulted in clean insertion of CS_2 into the Pd-Pd bond. The authors hypothesized that a CO_2 insertion product (**10b**) may be kinetically accessible but thermodynamically unfavorable. They anticipated that CO_2 conversion may be possible by a subsequent favorable reaction of the presumed Pd–O bonded

intermediate with a Me_3Si-X reagent. Therefore, they tested reaction of a C_6D_6 solution of **10a** with CO_2 (1 atm) in the presence of either Me_3SiCl or Me_3SiOTf. Heating of these two mixtures at 80 °C for 18 h resulted in complete utilization of **10a** and the formation of $(^FPNP)PdCl$ (**10c**) and $(^FPNP)PdOTf$ (**10e**) as major Pd products in 70% and 90% yield, respectively (Scheme 10). In both the reactions, $(Me_3Si)_2O$ was detected by ^1H NMR spectroscopy. Formation of $(Me_3Si)_2O$ and **10c** or **10e** suggests that CO may be the other major product.
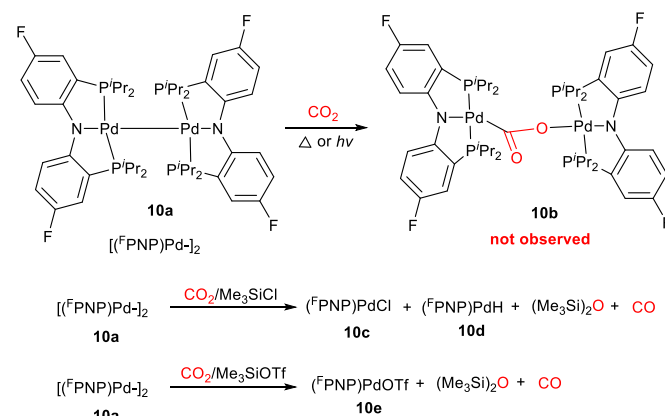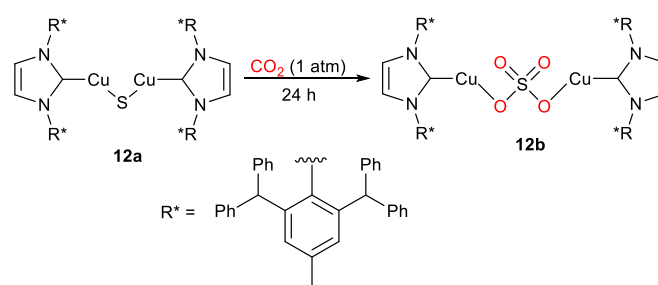
Scheme 10. Unsuccessful activation of CO_2 by a Pd(I) dimer and conversion of CO_2 to CO by Pd(I)-Pd(I)/Me_3SiX

Qu and co-workers studied CO_2 reactivity of the thiolate-bridged dicobalt(II) complex $[Cp^*Co(\mu$-SEt$)_2CoCp^*]$ (**11a**).[38] Treating **11a** with 1 atmosphere of CO_2 at room temperature or elevated temperature gave no reaction. Remarkably, upon addition of 0.5 equiv. of O_2 into the reaction mixture, CO_2 was readily inserted by the two cobalt centres to form a thiolate-bridged dicobalt carbonate complex $[Cp^*Co(\mu$-SEt$)_2(\mu$-η^1:η^1-$CO_3)CoCp^*]$ (**11b**) in excellent yield (90%) (Scheme 11). In the infrared (IR) spectrum, an absorbance at 1617 cm^{-1} with a medium intensity can be assigned to the vibrational mode ν(C=O) of the carbonate fragment, whereas two other strong absorption peaks at 1537 and 1444 cm^{-1} are for ν(C-O) of the carbonate moiety. They investigated the feasibility of CO_2 functionalization in this thiolate-bridged dicobalt(II) system. Accordingly, in presence of 1 equiv of $[FeCp_2][PF_6]$ as a one-electron oxidant, treatment of complex **11a** with stoichiometric primary alcohols ROH (R =Me, Et) in 1 atm CO_2 in CH_2Cl_2 from -78 °C to room temperature afforded the corresponding monoalkyl carbonate-bridged dicobalt complexes $[Cp^*Co(\mu$-SEt$)_2(\mu$-η^1:η^1-$O_2COR)CoCp^*][PF_6]$: [**11c**][PF$_6$], R = Me; [**11d**][PF$_6$], R = Et) in excellent yields (Scheme 11). Further, they showed the reactivity of **11b** toward the protonation and methylation.[38]
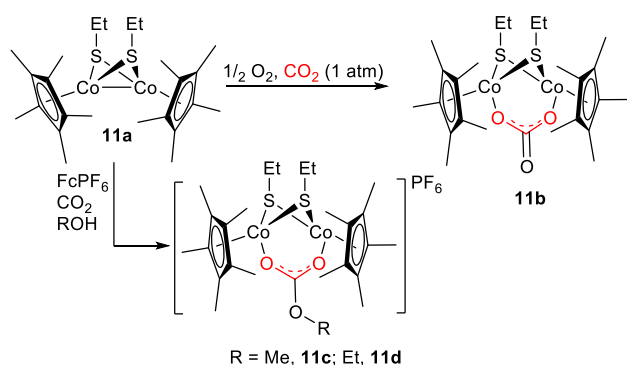
Scheme 11. Activation of CO_2 by bimetallic Co complex

Scheme 12. Reaction of CO_2 with a bimetallic Cu(I) sulfide complex

In 2018, our group reported the activation of CO_2 with a [$Cu_2(\mu\text{-}S)$] complex previously synthesized by Hillhouse and coworkers.[39] Reaction of [(IPr*)Cu]$_2$(μ-S) (**12a**) with 1 atm CO_2 at room temperature (Scheme 12) provided similar results to the N_2O reaction (*vide infra*). [(IPr*)Cu]$_2$(μ-SO$_4$)] (**12b**) was isolated as a major product and IPr*·CO_2 as a minor product along with three unidentified products in trace quantities.[40] In contrast to the N_2O case, addition of PPh_3 had no impact on reaction outcome. The initial intermediate of CO_2 activation, the bridging thiocarbonate species [(IPr*)Cu]$_2$(μ-SCO$_2$), was modeled computationally but could not be observed experimentally. This intermediate was proposed to decarbonylate to form [(IPr*)Cu]$_2$(μ-SO), which would subsequently undergo further oxidation by CO_2.

In nature, CO dehydrogenase (CODH) enzymes catalyze interconversion of CO and CO_2: $CO + H_2O \rightleftharpoons CO_2 + 2H^+ + 2e^-$. Among CODHs, the Ni-based enzymes utilize a common active site, the C-cluster, to mediate this transformation (Figure 1a). The C-cluster includes a distorted $NiFe_3S_4$-cubane that is coordinated via sulfide to an external iron site that plays a critical role in catalysis.[9] Lu group described synthesis of an anionic Ni-Fe complex **13a**, in which Ni is in the -1 oxidation state, and used **13a** convert CO_2 to CO_3^{2-}. They presumed that the anionic Ni-Fe species first bound CO_2 as the key intermediate in the overall process to reductively cleave CO_2 to form carbonate and Ni-bound carbonyl adduct **13b**. To peruse the reactivity analogous to CODH they checked the reactivity of the reduced Ni-Fe complexes with CO_2.[41] Upon exposure of **13a** and 2 equiv of benzo-15-crown-5 (B-15-C-5) in THF-d_8 to 1 atm CO_2 at ambient temperature, a new paramagnetic species was quantitatively formed (Scheme 13). This intermediate is stable for a few hours at room temperature. Further heating to 50 °C resulted in a final mixture of **13c** (major), anionic Ni-Fe carbonyl complex **13b** (minor), and CO_3^{2-}. In the absence of B-15-C-5, the same product mixture formed at 40 °C, but no intermediate was detected.
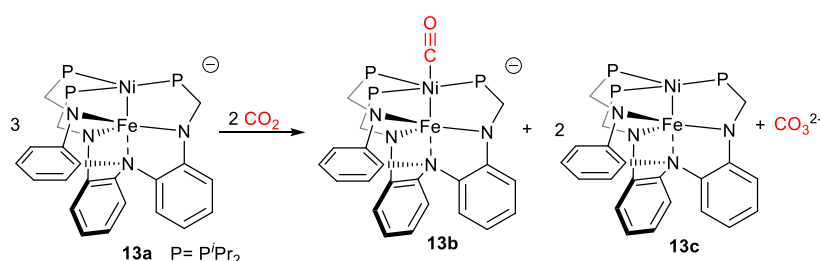
Scheme 13. Disproportionation of CO_2 by a Ni-Fe heterobimetallic complex

Transition metal/main group bimetallic complexes

The concept of Z-type Lewis acids (LA) binding to transition metals (TM) as σ-acceptor ligands is now a well-known strategy to modulate a transition metal's properties. The reaction of the geminal PAl ligand [Mes$_2$PC(=CHPh)Al^{t}Bu$_2$] with a Pt(0) source resulted the T-shape Pt-Al complex **14a** in 64% isolated yield.[42] X-ray diffraction analysis and DFT calculations revealed significant Pt→Al interaction in **14a**, despite the strained four-

membered metallacycle. The reaction of **14a** with CO_2 was carried out at room temperature. The reaction was completed after 17 h, and complex **14b** was isolated in 45% yield as a white solid (Scheme 14). DFT calculations found that the reaction of the masked Pt,Al-based FLP **14a** with CO_2 is exergonic by 5.5 kcal mol^{-1} ($\Delta H = -11.3$ kcal mol^{-1}). Nevertheless, **14b** was found to slowly decompose in vacuum as well as in solution into unidentified products. The molecular structure revealed CO_2 insertion into the Pt-Al bond, forming the first example of η^1-

CO_2 coordination to a Group 10 metal (which otherwise tend to form η^2-CO_2 adducts).
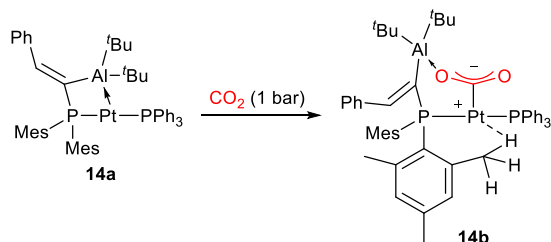
Scheme 14. Activation of CO_2 by a Pt-Al bimetallic complex

Lu group showed that a Ni complex supported by a Lewis acidic Ga(III) (**15a**) catalyzes direct CO_2 hydrogenation to formate at ambient temperature with high turnover numbers (3500) and high turnover frequency (9700 h^{-1}).[43] The anionic Ni(0) hydride, [VkdH][HNiGaL] (**15a**) (Vkd = 2,8,9-triisopropyl-2,5,8,9-tetraaza-1-phosphabicyclo[3.3.3]-undecane), was generated *in situ* by reacting a THF-d_8 solution of NiGaL (L = tris(phosphinoamido)amine ligand) with 3-5 equiv of Vkd and 1 atm of H_2. Here the strong Ni→Ga dative interaction helps to stabilize the electron-rich, anionic Ni-H moiety, which was found to be the most hydridic Ni-H complex ever reported ($\Delta G^\circ_{H-} \approx 31$ kcal/mol). The importance of the Lewis acidic Ga(III) support was further emphasized via comparison with NiLH$_3$, which was not reactive towards CO_2 hydrogenation. The formate species **15b** was generated *in situ* by exposure to 1 atm of CO_2 (Scheme 15). The solid-state structure of the resulting complex shows η^1-O formate ligand and Ni-Ga bond length is 2.3789(5) Å, which is essentially identical to that of **15a**.
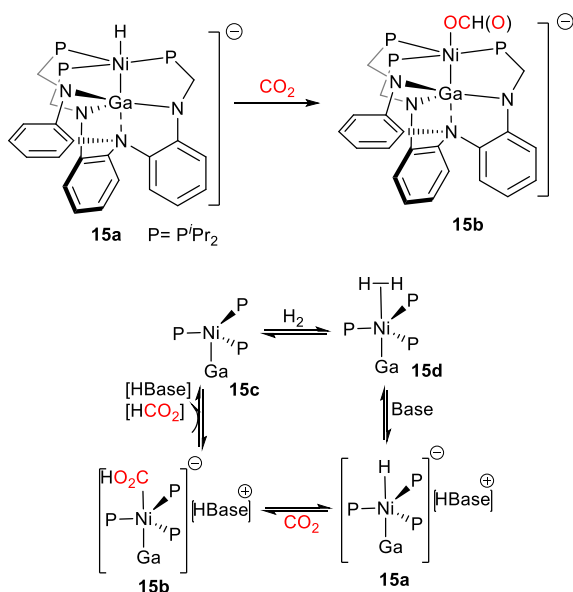

Scheme 15. Hydrogenation of CO_2 with a Ni-Ga bimetallic complex

Aldridge and Goicoechea group described the synthesis of heterobimetallic complex (NON)AlAuP^{t}Bu$_3$ (NON = 4,5-bis(2,6-diisopropylanilido)-2,7-di-tert-butyl-9,9-dimethylxanthene) featuring strongly polarized Au$^{\delta-}$-Al$^{\delta+}$ bond.[44] They explored the

reactivity of this complex with heteroallenes such as CO_2, in which the authors propose that the gold centre acts as a nucleophile. CO_2 (1 atm) was added to a toluene solution of **16a** at room temperature, leading to clean formation of the insertion product (NON)Al(O$_2$C)AuP^{t}Bu$_3$ (**16d**) (Scheme 16). The structure was confirmed crystallographically and it shows single molecule of CO_2 reductively inserted into the Al–Au bond. A recent computational study disputes the characterization of the reaction pathway as involving nucleophilic gold and electrophilic aluminum, instead favoring reaction with CO_2 through an electronic state with metal-metal diradical character.[45]

The same group also synthesized coinage metal aluminyl complexes (NON)AlMP^{t}Bu$_3$ (M= Ag (**16b**), Ag (**16c**)), featuring M-Al covalent bonds.[46] The bimetallic complex (NON)AlAgP^{t}Bu$_3$ (**16b**) readily reacts with CO_2, resulting insertion of CO_2 into the unsupported Ag-Al bond to give system containing a Ag(CO_2)Al bridging unit **16e** (Scheme 16). Whereas (NON)Al(O$_2$C)AuP^{t}Bu$_3$ is inert to further reaction with CO_2, the silver analogue reacts slowly with CO_2 at high temperature to give the corresponding carbonate complex **16f** along with elimination of CO (Scheme 16). In case of copper aluminyl complex (NON)AlCuP^{t}Bu$_3$ (**16c**) reaction with CO_2 resulted corresponding carbonate complex **16g** and even at -78 °C with no observable intermediate. The authors proposed a mechanism for carbonate formation that proceeds via elimination of CO from (NON)Al(O$_2$C)MP^{t}Bu$_3$ (M= Cu, Ag) to give a reactive M-O-Al species that rapidly reacts further with CO_2.
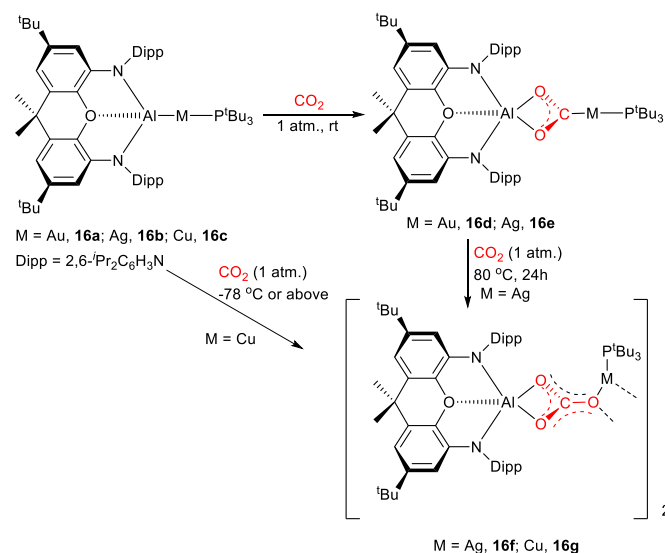
Scheme 16. Reaction of CO_2 with Al-M (M = Cu, Ag, Au) complexes

Hill and McMullin groups recently reported two heterobimetallic Cu-Al complexes; LCuAl(SiN^{Dipp}) where L = N,N'-diisopropyl-4,5-dimethylimidazol-2-ylidene (NHC^{iPr}) (**17a**) or 1-(2,6-diisoprorpylphenyl)-3,3,5,5-tetramethyl-pyrrolidin-2-ylidine (^{Me2}CAAC) (**17b**), featuring reactivity toward CO_2.[47] Exposure to isotopically labelled $^{13}CO_2$ resulted in the rapid formation of the metallacarboxylate complexes, **17c** and **17d**, respectively (Scheme 17). The structure **17d** was confirmed by

X-ray diffraction analysis; however, the crystal structure of **17c** could not be obtained. The ^{13}C NMR spectra for **17c** and **17d** suggested similar structures because the characteristics low-field resonances indicative of Cu-CO_2 bonding were located at comparable chemical shifts of 236.2 and 234.9 ppm, respectively.
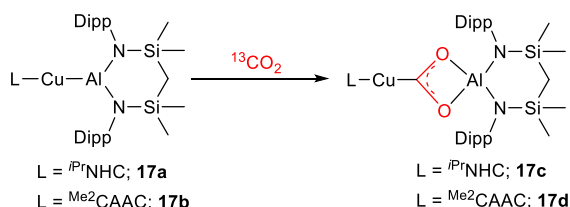
Scheme 17. Reaction of CO_2 with Al-Cu complexes

Camp and co-workers described a unique example where an alkylaluminum Lewis acid induced umpolung character to an iridium centre, switching iridium half-metallocenes into nucleophiles through the formation of polarized $Ir^{\delta-}$-$Al^{\delta+}$ pairs.[48] Reaction of diisobutyl(3,5-di-tert-butyl-4-hydroxytoluene)aluminum $[Al(^{i}Bu)_2(OAr)]$, with Cp^*IrH_4 at room temperature resulted in the formation of the heterobimetallic complex $[Cp^*IrH_3Al(^{i}Bu)(OAr)]$ (**18**) in 72% isolated yield. Complex **18** can form an adduct with pyridine resulting $[Cp^*IrH_3Al(^{i}Bu)(OAr)(Py)]$ (**18a**) in 68% isolated yield. Next, they investigated the reactivity of these $Ir^{\delta-}$-$Al^{\delta+}$ derivatives toward CO_2. The reaction of **18** with CO_2 proceeds at room temperature and produces a complex mixture of species. From the mixture they identified $Cp^*Ir(CO)H_2$ and Cp^*IrH_4 among some unidentified products. Treatment of Lewis acid adduct **18a** with CO_2 leads to the cooperative reductive cleavage of CO_2 (Scheme 18), affording the iridium carbonyl species $Cp^*Ir(CO)H_2$ (**18b**), iridium hydride Cp^*IrH_4, and the aluminum-oxo complex $[(^{i}Bu)(OAr)Al(Py)]_2(\mu$-O) (**18c**), which is isolated in 86% yield (Scheme 18). In these reactions, the Ir(III) center acts as a nucleophile, which behavior is unusual for a d^6 Ir(III) complex. DFT calculations were consistent with cooperative CO_2 activation via concerted transition state.
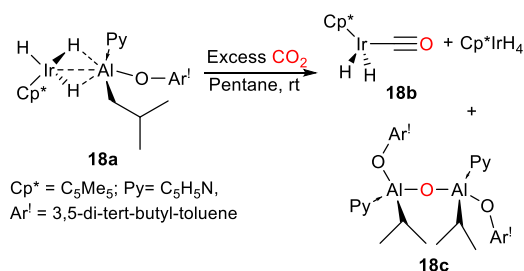
Scheme 18. Cooperative activation of CO_2 by a Lewis acid-bound Ir(III) complex

Very recently our group reported cooperative activation of CO_2 by a heterobimetallic Al-Fe complex.[49] The complex, L(Me)Al-Fp (**19a**) (L = $HC\{(CMe)(2,6-^{i}Pr_2C_6H_3N)\}_2$, Fp $=FeCp(CO)_2$), was found to react with CO_2 cleanly at room temperature and 1 atmosphere pressure. The CO_2 inserted product $L(Me)Al(O_2C)Fp$ (**19b**) was isolated as a white solid in excellent yield (Scheme 19). Detailed kinetic and theoretical

studies on CO_2 insertion reaction indicate an unusual radical pair mechanism: the Al-Fe bond dissociates to generate [L(Me)Al]· and [Fp]· intermediates, followed by CO_2 coordination to Al and then radical rebound of [Fp]·.
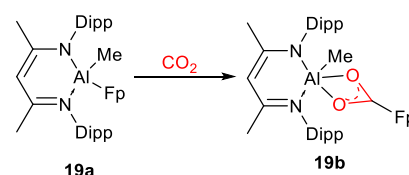
Scheme 19. Activation of CO_2 by an Al-Fe complex

Main group bimetallic complexes

There were no previous reports on the reduction of CO_2 to CO using well defined s-block element complexes until 2013, when the Jones group reported reactivity of dimeric magnesium(I) complexes towards CO_2. A dimeric magnesium(I) complex was found to react with CO_2 to give the Mg(II) carbonate complex and CO via a reductive disproportionation process.[50] Addition of two equivalents of CO_2 to a yellow toluene solution of $[(LMg)_2]$ (**20a**) (L = $HC\{(CMe)(2,6-^{i}Pr_2C_6H_3N)\}_2$,) at room temperature led to the rapid discoloration of the solution, and the formation of the carbonate bridged magnesium(II) compound, $[\{LMg\}_2(\mu$-κ^2:κ^2-$CO_3)]$ (**20b**) (Scheme 20). Formation of CO as a byproduct was confirmed by carrying out the reaction of $[(LMg)_2]$ with $^{13}CO_2$. In ^{13}C NMR spectroscopy, the most prominent signals appeared at δ 184.5 and 168.1 ppm, were assigned to ^{13}CO and the ^{13}C enriched carbonate ligand of **20b**, respectively. It is worth to mentioning that the reaction of $[(LMg)_2]$ with a large excess of CO_2 led to an intractable mixture of many products at room temperature.
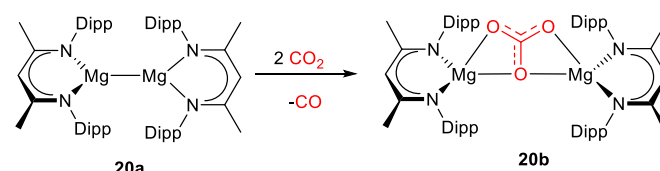
Scheme 20. Disproprtionation of CO_2 by a Mg(I) dimer

Since the reaction of **20a** with excess CO_2 was difficult to control, the authors hypothesized that the nucleophilic γ-backbone carbon center of the β-diketiminate ligand can attack the electrophilic CO_2 molecule, as has been found for other magnesium β-diketiminate complexes,[51] to lead to ligand decomposition pathways. To prevent such secondary reactivity, they prepared a series of four-coordinate diimine–enolato magnesium(I) complexes by reacting β-diketiminate stabilized Mg(I) dimers with $O=C=CPh_2$.[52] The reaction of one of the aforementioned complex with excesses CO_2 was readily controlled, and the nature of the products was shown to be temperature dependent. The reaction of diimine–enolato magnesium(I) dimer (**21a**) with excess CO_2 was carried out at room temperature. ^1H NMR spectrum analysis of reaction

mixture showed formation of magnesium carbonate and oxalate products, **21b** and **21c** respectively, in an approximately 60:40 ratio (Scheme 21). When the reaction was carried out at 60 °C, quantitatively the carbonate **21b** was formed. In contrast, when the reaction was carried out at -60 °C, quantitatively the oxalate complex **21c** was formed, and there was no evidence of CO formation. Interestingly, the temperature-dependent selectivity of the reaction of **21a** with excess CO_2 indicates that the carbonate complex **21b** is the thermodynamic product, whereas the oxalate complex **21c** is the kinetic product.
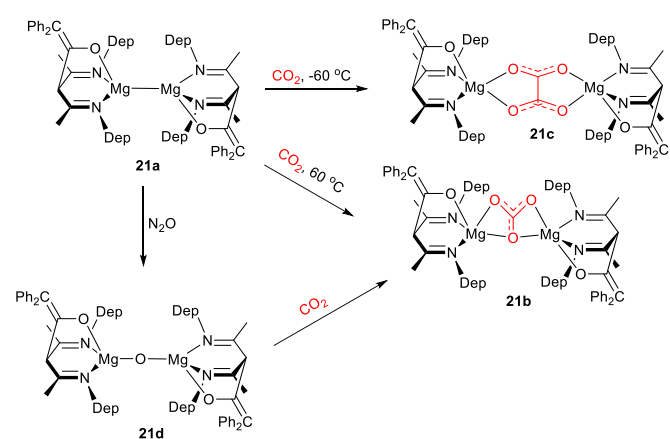

Scheme 21. Temperature-dependent reactivity of CO_2 with a Mg(I) dimer

Recently Inoue group reported CO_2 fixation and catalytic reduction by silyl-substituted dialumene.[53] Addition of CO_2 (1 atm) to the purple solution of dialumene (**22a**) at -78 °C, then warming the reaction mixture to -30 °C resulted in color change from deep purple to yellow. **22b** was isolated as a yellow solid in quantitative yield (Scheme 22). XRD analysis revealed that CO_2 fixation had occurred via [2+2] cycloaddition to the Al=Al double bond. **22b** was found to be relatively stable in the solid state and can be stored in an inert atmosphere at room temperature for a month without any signs of decomposition. In C_6D_6 or [D_8]THF solution at room temperature, further color change to a dark orange was observed after 18 h. NMR spectra showed the formation of a new species, with a downfield signal in the ^{13}C NMR spectrum at δ 276.0 ppm. Heating the solution of **22b** at 50 °C for 1h resulted in a dark red solution, and after crystallization **22c** was isolated in 20% yield (Scheme 22). XRD analysis revealed that **22c** consists of bridging carbonyl and oxo units between the two Al centres. Surprisingly, when a C_6D_6 solution of **22b** was heated at 50 °C under an atmosphere of CO_2, initially **22c** formed but then converted to a colorless solution, rather than the expected red solution for the formation of **22c** (Scheme 22). The ^{13}C NMR spectrum of the colorless product revealed new signals at δ154.4 ppm and 184.4 ppm, indicating formation of carbonate and CO, respectively. XRD analysis showed that compound **22d** consists of a six-membered ring containing a bridging carbonate group and a bridging oxygen atom between the two aluminum centers.
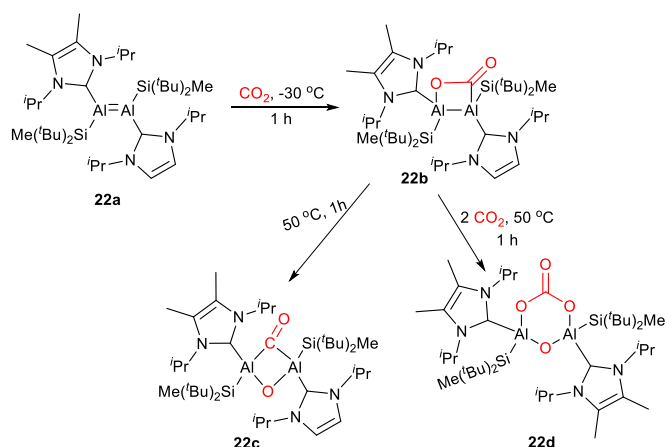
Scheme 22. CO_2 reactivity of a silyl-substituted dialumene

By replacing silyl substituents by aryl groups in the dialumene, the same group observed enhanced reactivity due to **23a** being supported by higher flexibility as well as enhanced polarization of the dialuminium bond. Reaction of CO_2 with **23a** resulted in immediate color change from black to colorless. Examining the ^{13}C NMR spectrum disclosed the presence of CO (δ 184.4 ppm) and CO_3 (δ 159.12 ppm), suggesting the formation of the carbonate complex **23b**.[54] Here attempt to isolate a [2+2] cycloaddition product was unsuccessful as it rapidly converted to compound **23b** (Scheme 23). Both the silyl- and aryl-substituted complexes with oxo bridges (**23d** and **23e**) also react with CO_2, resulting in carbonate complexes.[54]
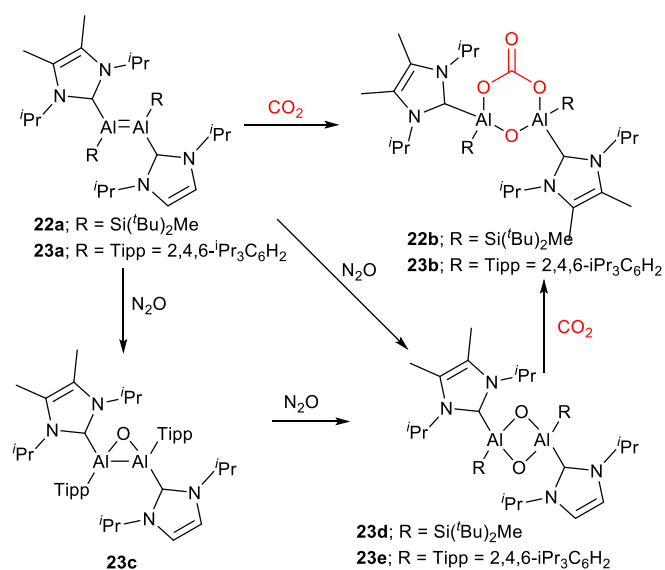
Scheme 23. Reaction of CO_2 with silyl- and aryl-substituted dialumenes

Next, the Inoue group attempted catalytic reduction of CO_2 with pinacolborane mediated by dialumene complexes. Silyl-substituted complex **22a** was found to catalyze the reduction of CO_2 with HBpin (HBpin = pinacolborane) selectively to the formic acid equivalent (**24a**, Scheme 24) in 86% yield.[53] Although this reaction proceeds at room temperature, it required up to 1 week and 10 mol% of **22a**. On the contrary, 5 mol% of catalyst **23a** was used for hydroboration of CO_2 at room

temperature. ^1H and ^{11}B NMR spectra showed the consumption of HBpin in less than 3 days along with the formation of new B-O containing species. The ^1H NMR spectrum of reaction mixture showed the formation of further reduced species (**24b**, **24c**, **24d**, Scheme 24), suggesting that **23a** is not only more catalytically active but also proceeds through a different mechanism.[54]
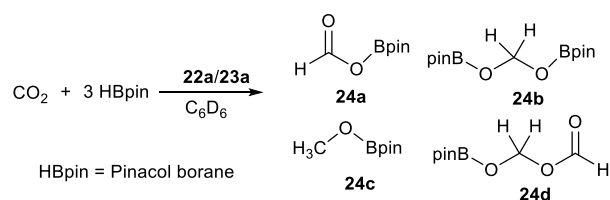
Scheme 24. Catalytic reduction of CO_2 with pinacolborane mediated by dialumene complexes

Bimetallic f-element complexes

In 2010, Meyer's group reported carbonate formation from CO_2 via reductive processes using U(III) complexes.[55] They also demonstrated the mechanism for this reductive process. For their study they used an U(III) complex with a new tripodal ligand system [(($^{tBu}ArO)_3$mes)U] (**25a**) and another one with a single nitrogen anchor [(($^{Ad}ArO)_3$N)U] (**25b**). Accordingly, reacting a deep purple solution of **25a** in toluene with excess CO_2 (1 atm) at room temperature resulted in formation of a pale-yellow solution within 10 min. The yellow solid was isolated and characterized as the dinuclear U(IV)/U(IV) bridging carbonate complex [{(($^{tBu}ArO)_3$mes)U}$_2$(μ-κ^2:κ^2-CO_3)] (**25e**) (Scheme 25).[55] Similarly, a brown suspension of **25b** in DME was reacted with an excess of CO_2 (1 atm), and immediately a green product was formed. The green solids were characterized as the U(IV)/U(IV) bridging carbonate complex with different coordination mode: [{(($^{Ad}ArO)_3$N)U}$_2$(μ-η^1:κ^2-CO_3)] (**25f**) (Scheme 25). For mechanistic studies, reactions of **25a** and **25b** with 1 atm of N_2O were carried out, and bridging oxo species [{(($^{tBu}ArO)_3$mes)U}$_2$(μ-O)] (**25c**) and [{(($^{Ad}ArO)_3$N)U}$_2$(μ-O)] (**25d**) were formed (Scheme 25, Path B). Later, reactions of **25c** and **25d** with 1 atm CO_2 resulted in the uranium bridging carbonate complexes **25e** and **25f**, respectively (Scheme 25). These observations are consistent with bridging oxo species **25c** and **25d** being initially formed from CO_2 with simultaneous release of CO, followed by nucleophilic attack at CO_2 by the bridging oxo ligand (Scheme 25, Path A).
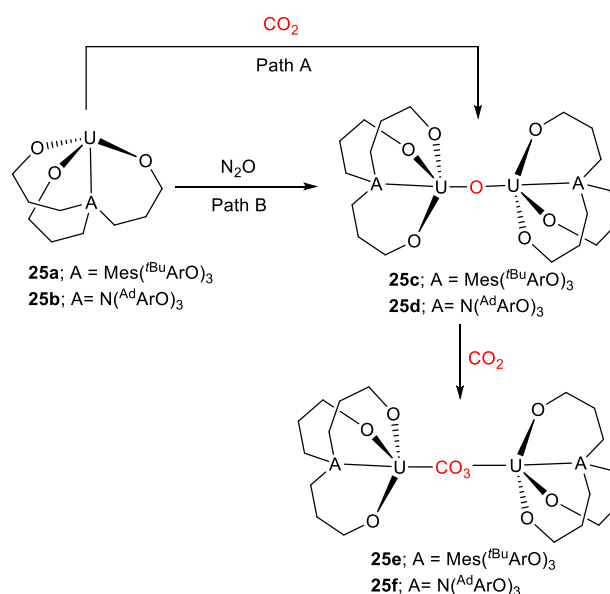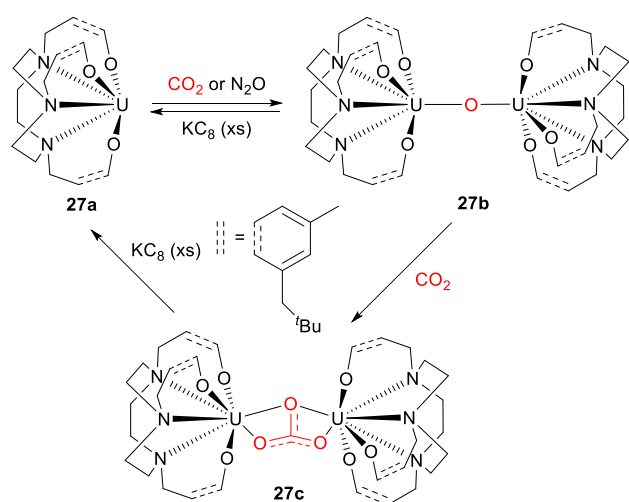

Scheme 25. Activation of CO_2 by U(III) complexes

DFT analysis indicated that, while the reaction between **25a** and CO_2 to form **25e** is thermodynamically favourable and kinetically accessible,[56] a hypothetical competing pathway to form a μ-oxalate complex is prohibited due to the high activation barrier. Later, the same group achieved access to uranium oxalate complex [{(($^{nP,Me}ArO)_3$tacn)$_3$U^{IV}}$_2$(μ-κ^2: κ^2-C_2O_4) (**26b**) through CO_2 activation by trivalent uranium complex [(($^{nP,Me}ArO)_3$tacn)$_3$U^{III}] (**26a**) in the presence of KC_8 (Scheme 26).[57] Use of THF solvent was found to be critical to formation of **26b**, possibly due to slow KC_8 reduction in this medium. Besides **26b**, a similar carbonate complex to **25e** was obtained as a minor product.
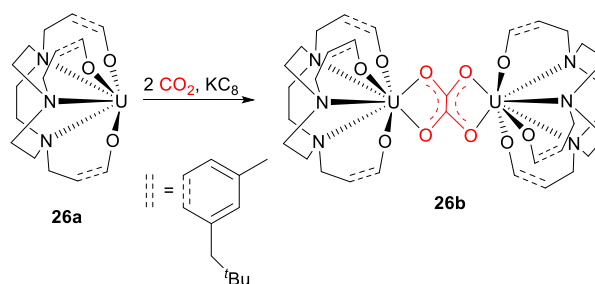
Scheme 26. Activation of CO_2 by U(III) complexes

Later, Meyer's group also reported the synthesis of a dinuclear U^{IV} complex from the reaction between mononuclear [($^{Neop,Me}ArO)_3$tacnU^{III}] (**27a**) and one equivalent of CO_2.[58] Similar to their prior work,[55] the dinuclear U^{IV} complex [{(($^{Neop,Me}ArO)_3$tacnU}$_2$(μ-O)] (**27b**) could also be obtained from exposure of **27a** to N_2O atmosphere. In the presence of excess CO_2, complex **27b** accordingly formed carbonate complex [{(($^{Neop,Me}ArO)_3$tacnU}$_2$(μ-CO_3)] (**27c**) which was further reduced by KC_8 to complex **27a** (Scheme 27). Thus, a closed synthetic cycle for CO_2 reduction was achieved.

Scheme 27. Activation of CO_2 by U complexes

Evans and co-workers reported a Sc^{2+} analogue was found to react rapidly with CO_2.[59] Addition of 1 atm of CO_2 to *in-situ* prepared [K(18-c-6)][$(R_2N)_3Sc$] (**28a**) resulted in immediate color change to colorless (R = $SiMe_3$). The IR spectrum of the crude product indicated the presence of two CO_2-derived products. One was the colorless bridging oxalate complex, [$K_2(18-c-6)_3$]{[$(R_2N)_3Sc]_2(\mu-C_2O_4-\kappa^1O:\kappa^1O'')$] (**28c**). Subsequent crystallization revealed the other product to be [$(R_2N)_3Sc(\mu-OCO-\kappa^1O:\kappa^1O')K(18-c-6)]_n$ (**28b**) (Scheme 28). XRD analysis revealed that the latter complex is polymeric with the repeating units connected by a [K(18-c-6)]$^+$ unit and a methyl group of the NR_2^- ligand. The assignment of a linear Sc-O=C=O-K unit is surprising considering that CO_2 bending should occur upon electron transfer from Sc(II) into the π^* manifold, and so further investigation is warranted.
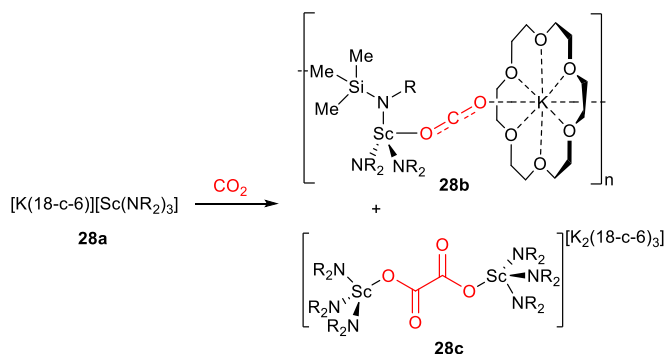

Scheme 28. Reaction of CO_2 with a Sc(II) complex (R = $SiMe_3$)

In 2012, Mazzanti and co-workers studied a siloxide-supported trivalent uranium complex, [{$U(OSi(O^tBu)_3)_2(\mu-OSi(O^tBu)_3)$}$_2$] (**29a**), and its reactivity towards CO_2.[60] The formation of dinuclear U^{IV} carbonate complex [{$U(OSi(O^tBu)_3)_3$}$_2${$\mu-\kappa^1: \kappa^2-CO_3$}] (**29b**) was obtained when the solution of **29a** in hexane was exposed to CO_2 for 6 h (Scheme 29). Byproduct CO was detected by ^{13}C NMR spectroscopy and chemically trapped by vanadocene. During the reaction, minor U^{IV} complex [$U(OSi(O^tBu)_3)_4$] (**29c**) was identified ^1H NMR spectroscopy and X-ray crystallography. The ratio between **29b**

and **29c** was 2.5:1 after the reaction was complete. Complex **29b** was decomposed to yield **29c** over extended time periods, indicating slow ligand re-distribution of complex **29b** to form **29c**. Gibbs free energy calculations indicated that the concerted one-electron reduction of two molecules of CO_2 was kinetically favourable (14.5 kcal mol^{-1}) compared to the formation of the oxo intermediate (23.8 kcal mol^{-1}). Another possibility involving formation of a six-membered ring intermediate that spontaneously releases CO to form **29c** could not be ruled out.
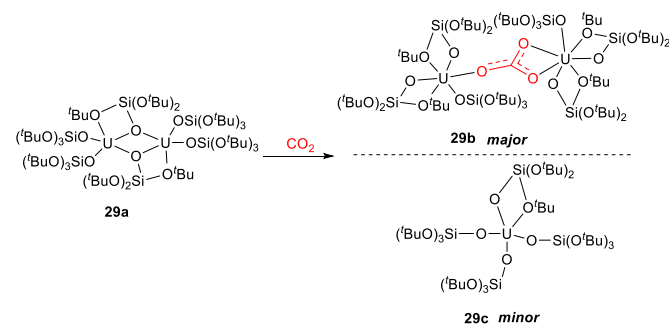
Scheme 29. Activation of CO_2 by a bimetallic U(III) system

Then, they described multimetallic cooperative effect in the reduction of CO_2.[61] They used potassium and uranium bimetallic systems for reduction of CO_2. The reaction of [$U(OSi(O^tBu)_3)_4K$] (**30a**) with 1 atm of CO_2 in toluene at room temperature afforded cleanly the terminal oxo pentavalent uranium complex [$UO(OSi(O^tBu)_3)_4K$] (**30b**) in 77% yield with CO as a byproduct (Scheme 30; left). This was the first example of a uranium(V) terminal oxo complex to be obtained from the two-electron reductive cleavage of CO_2. To investigate whether the presence of potassium plays any important role in the reaction, they studied the reaction of the analogous ion-paired system [K(18-c-6)][$U(OSi(O^tBu)_3)_4$] **30c** with 1 atm of CO_2. The reaction occurred instantly at room temperature and evolution of CO was observed. Crystallization of the reaction mixture in toluene formed pale pink single crystals of [K(18-c-6)][KU($\mu-\kappa^1:\kappa^2-CO_3$)(OSi(O^tBu)_3)_4$] (**30d**) (Scheme 30; right). The observation of gaseous CO and the isolation of the carbonate complex (**30d**) confirmed [K(18-c-6)][$U(OSi(O^tBu)_3)_4$] facilitates the disproportionation of CO_2. Thus, this study showed that CO_2 reduction selectivity can be controlled by the presence or absence of a coordinated alkali-metal ion bound near the U(III) center. The DFT-optimized structure of **30a**·CO_2 indicated that negative charge on the reduced CO_2 moiety is stabilized by coordination to both the uranium and the potassium centers, thus supporting the presence of cooperative effect of the two metal centres in the conversion of CO_2.
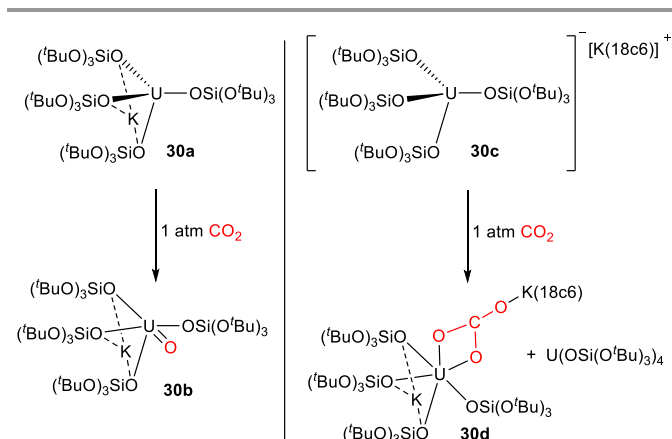
**Scheme 30.** Activation of CO_2 by a bimetallic K/U(III) complex

Neif, Evans, and Maron groups investigated the mechanism of CO_2 activation by the binuclear complex, $[Cp*_2Sm]_2(\mu\text{-}O)$ (**31a**). The oxide complex **31a** reacted with CO_2 for 1 h in benzene, and subsequent addition of THF resulted in $[\{(C_5Me_5)_2Sm(THF)\}_2(\mu\text{-}\kappa^1:\kappa^2\text{-}CO_3)]$, **31b** (Scheme 31). Three different possible pathways were explored computationally and revealed that a common initial intermediate was a binuclear Sm^{III} complex, $[\{(C_5Me_5)_2Sm\}_2(\mu\text{-}\eta^2:\eta^1\text{-}CO_2)]$.[62]
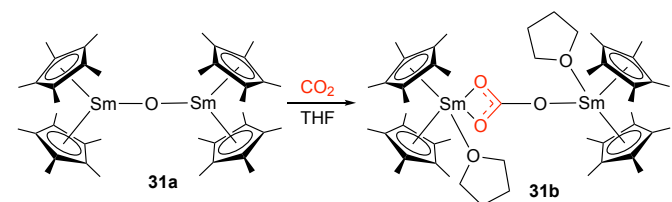

Scheme 31. Activation of CO_2 by a bimetallic Sm complex

Nocton and coworkers reported the reductive disproportion of CO_2 using bulky divalent samarium complexes. Accordingly, the reaction of both Cp^{tt}_2Sm (Cp^{tt} = 1,3-$(^tBu)_2(C_5H_3)$; **32a**) and Cp^{ttt}_2Sm ((Cp^{ttt} = 1,2,4-$(^tBu)_3(C_5H_2)$; **32c**)) with CO_2 (1 atm) were performed at low temperature in deuterated toluene.[63] Both reactions resulted immediate color changes, and structural analysis showed bridging carbonate (CO_3^{2-}) ligands between the two samarocene fragments in both cases, $[Cp^{tt}_2Sm]_2(\mu\text{-}CO_3)$ (**32b**) and $[Cp^{ttt}_2Sm]_2(\mu\text{-}CO_3)$ (**32d**) (Scheme 32). The coordination modes of the bridging carbonate ligands were found to be different when comparing structures of **32b** and **32d**. A combination of experimental and computational investigations was unable to distinguish between multiple possible mechanisms with roughly isoenergetic activation energies.
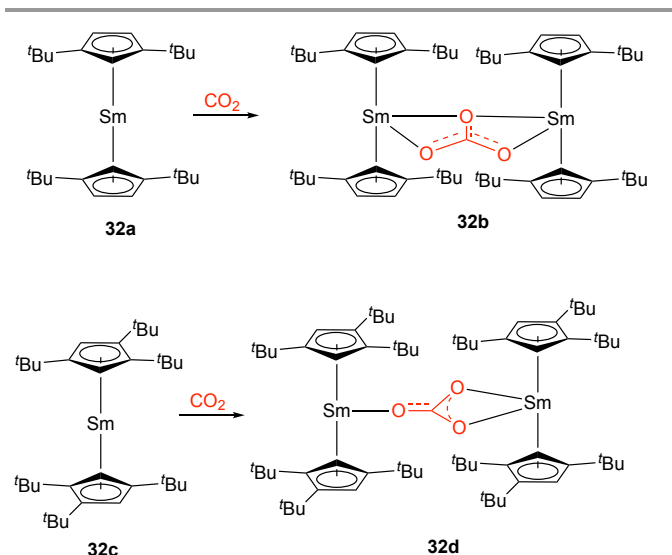
Scheme 32. Activation of CO_2 by a Sm complex

In 2016, Mills and Maron groups reported the first case of CO_2 reactivity by a thorium complex. Reaction of $[Th(Cp'')_3]$ (**33a**, $Cp''=\{C_5H_3(SiMe_3)_2\text{-}1,3\}$) with CO_2 afforded the mixed oxalate/carboxylate dithorium(IV) complex $[\{Th(Cp'')_2[\kappa^2\text{-}O_2C\{C_5H_3\text{-}3,3'\text{-}(SiMe_3)_2\}]\}_2(\mu\text{-}\kappa^2:\kappa^2\text{-}C_2O_4)]$ (**33b**) in 65% yield (Scheme 33).[64] The authors hypothesized that **33b** forms via $[\{Th(Cp'')_3\}(\mu\text{-}CO_2)]$ intermediate and further proposed that the bulky Cp'' ligands hinder the elimination of CO to form $[\{Th(Cp'')_3\}_2(\mu\text{-}O)]$, thus allowing a second CO_2 molecule to be incorporated to form oxalate. Reactions of **33a** with 1 or 2 equivalents of CO_2 or $^{13}CO_2$ at -78 °C were performed, and **33b** or **33b**-^{13}C were the only products identified by ^1H and ^{13}C NMR spectroscopy with no detected intermediates.
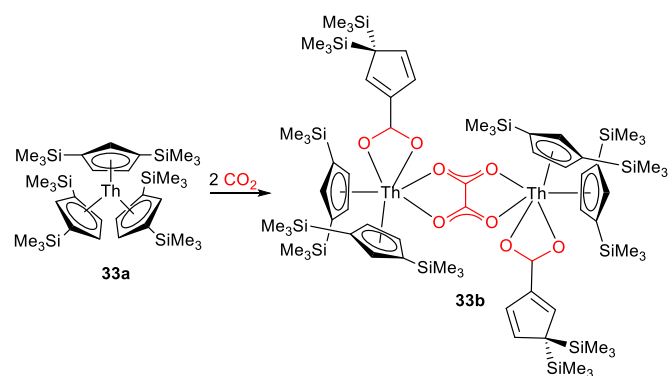
Scheme 33. Activation of CO_2 by a Th complex

In 2017, Cloke group performed the reaction of CO_2 with U(III) complex $[U(Cp*)(p\text{-}Me_2bp)]$ (**34a**, $Cp*$ = C_5Me_5; bp = bisphenol) at various conditions. When the reaction was carried out with supercritical CO_2 at high pressure and room temperature, a dinuclear uranium carbonate complex, $\{U(Cp*)(p\text{-}Me_2bp)\}_2(\mu\text{-}\eta^1:\eta^2\text{-}CO_3)$ (**34b**) formed cleanly and selectively (Scheme 34).[65] On the other hand when the reaction was carried out in conventional solvents using lower pressures of CO_2, a rare U(IV) oxalate complex $\{U(Cp*)(p\text{-}Me_2bp)\}_2(\mu\text{-}\kappa^2:\kappa^2\text{-}C_2O_2)$ (**34c**) was isolated along with **34b** (Scheme 34). The relative ratio of the two products is temperature dependent:

at low temperatures (−78 °C) oxalate formation is favoured, whereas at room temperature the carbonate is the major product.
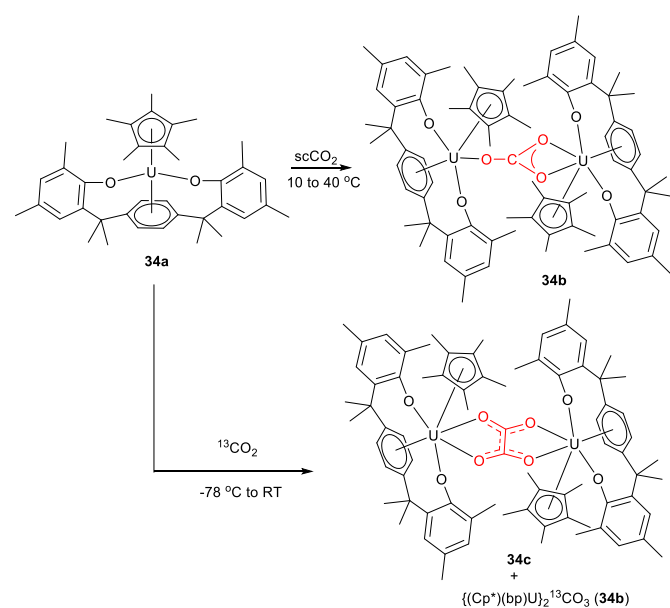
Scheme 34. Activation of CO_2 by a U(III) complex

Recently, Mazzanti group synthesized dinuclear homoleptic lanthanide(II) complexes supported by polydentate tris(tertbutoxy) siloxide ligand: [Yb_2L_4] (**35a**), and [Sm_2L_4] (**36a**)L = (O^t Bu)$_3$SiO⁻)). Complexes **35a** and **36a** reduced CO_2 under ambient conditions, resulting in carbonate and oxalate formation. When $^{13}CO_2$ was added to a C_6D_{12} solution of **35a** an immediate colour change was seen from brown to yellow. The ^{13}C NMR spectrum revealed the formation of carbonate (δ = 167.62 ppm) and oxalate (δ = 179.72 ppm) in a ratio of 50:1 with 94% total yield (Scheme 35). Similarly, when $^{13}CO_2$ (~5 equivalents) was added to a THF-d$_8$ solution of **35a**, an immediate colour change was observed from orange to yellow. The ^{13}C NMR spectrum of the reaction mixture showed the presence of free ^{13}CO and $^{13}CO_2$ as well as a signal at δ = 169.95 ppm that was assigned to the bound carbonate product (Scheme 35).[66]
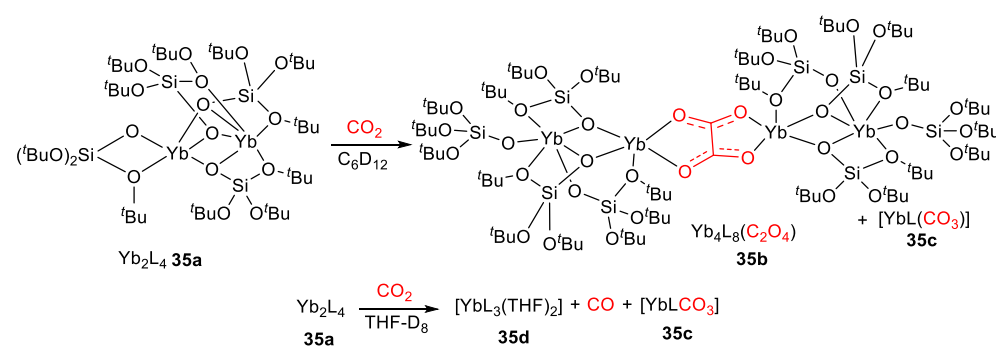
Scheme 35. Activation of CO_2 by a bimetallic Yb complex
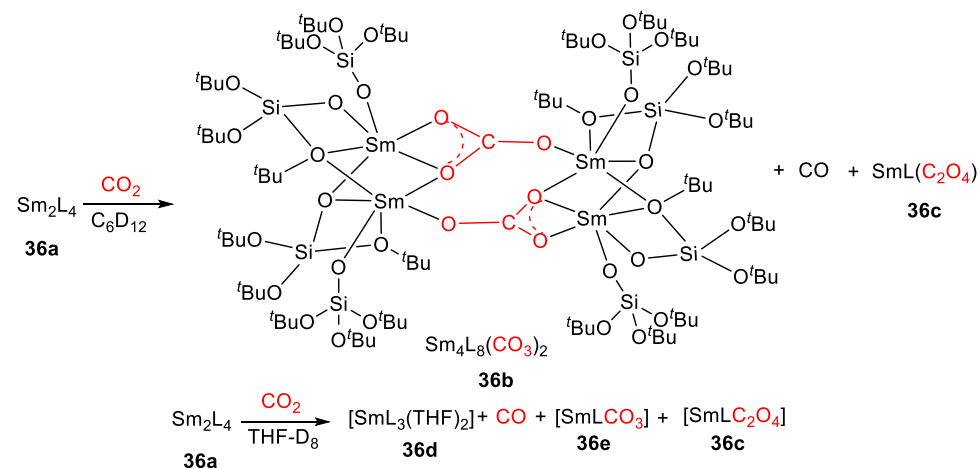
Scheme 36. Activation of CO_2 by a Sm complex

To assess the influence of the lanthanide ion on the reactivity they also investigated the reactivity of **36a**. The reaction of [Sm_2L_4] (**36a**) with $^{13}CO_2$ in C_6D_{12} afforded a slow colour change from dark brown to light brown. The ^{13}C NMR spectrum showed the presence

of excess $^{13}CO_2$ and free ^{13}CO as well as the presence of additional signals assigned to Sm-carbonate products (Scheme 36). When the same reaction was carried out in THF-d$_8$, an immediate colour change from dark brown to colourless was observed. The ^{13}C NMR spectrum

showed the presence of carbonate (**36b**) and oxalate (**36c**) in a 104:1 ratio and in 90% total yield (Scheme 36).[66] Computational studies confirmed that the formation of oxalate is preferred with respect to carbonate formation in the reaction of the dimeric lanthanide complexes with CO_2.

Bimetallic N$_2$O activation

Biomimetic multicopper complexes

Since N_2O is proposed to undergo cooperative activation at the Cu_Z site of N_2OR during bacterial denitrification (see Figure 2a), there has been great interest in designing synthetic multicopper platforms for N_2O activation.[67–69] In 2014, Torelli and coworkers reported the preparation and characterization of a dinuclear complex **37a** containing a mixed-valent [$Cu_2(\mu$-SR)] core and studied its reactivity towards N_2O reduction (Scheme 37).[70] This thiolate-bridged dicopper(I,II) cluster was found to reduce N_2O to N_2, resulting in fully oxidized Cu(II) metal centers with a double bridged [$Cu^{II}_2(\mu$-SR)(μ-OH)] core (**37b**). Mechanistic investigations revealed that, as expected for the two-electron reduction of N_2O, the reaction is second order with respect to the dicopper complex. Therefore, it was proposed that one dicopper complex is responsible for N_2O activation, while the other acts as a sacrificial redox reagent and proton donor. It is notable that a similar paradigm is proposed for Cu_Z: two Cu centers for N_2O binding and two Cu centers for electron transfer, i.e. Cu:N_2O ratio of 4:1. An intermediate N_2O adduct was characterized experimentally by UV-Vis spectrometry and ^{19}F NMR spectroscopy. DFT modeling indicated two possible coordination modes of approximately equal energy with either η^1-N or η^1-O N_2O binding, although the η^1-O isomer (**37c**) is more likely the reactive species that evolves N_2. Upon releasing N_2, a hypothetical [$Cu_2(\mu$-SR)(μ-O)]$^{2+}$ intermediate (**37d**) was proposed to form. Reaction of **37d** with a sacrificial equivalent of **37a** then produces two equivalents of **37b** by proton/electron transfers.
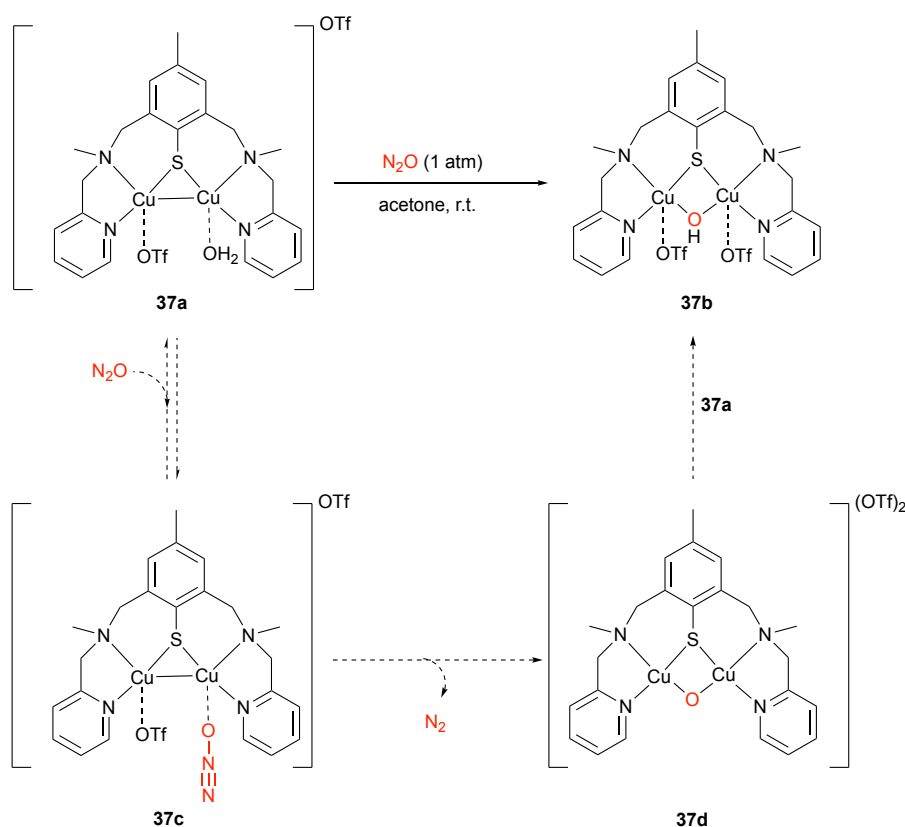
Scheme 37. Kinetic studies and theoretically proposed reaction pathway for N_2O reduction by a biomimetic dicopper(I,II) µ-thiolate complex.

In 2015-2016, our group reported a structurally faithful [$Cu_4(\mu_4$-S)] model for Cu_Z supported by formamidinate ligands and characterized it in its two-hole **38a** (formally 2Cu^I:2Cu^{II}) and one-hole **38b** (formally 3Cu^I:1Cu^{II}) redox states.[71,72] Exposure of **38b** to N_2O (1 atm) **38a** quantitatively, thus completing a synthetic cycle for N_2O reduction (Scheme 38).[72] The stoichiometric byproducts were proposed to be N_2, which was detected directly, and K_2O, which was trapped *ex situ* with electrophiles. In 2020, further experimental and computational studies of this system were reported.[73] By measuring the

reaction stoichiometry, it was determined that the overall two-electron reduction of N_2O required two equivalents of **38b**. Thus, it was proposed that one equivalent of the cluster is responsible for activating N_2O and the other for acting as an electron donor. Computational modeling of the reaction intermediates (Scheme 38) indicated an unexpected binding mode for N_2O across a Cu-S bond, rather than between multiple Cu sites as initially expected by analogy to Cu$_Z$. Consistent with direct participation of the μ_4-S^{2-} ligand in the redox transformation, XAS analysis of **38a** and **38b** indicated that the

sulfur center contributes significantly to the redox-active molecular orbital. This data represented the first spectroscopic interrogation of multiple redox levels of a conserved [4Cu:1S] cluster. Furthermore, the direct interaction of N_2O with the μ_4-S in this Cu$_Z$ model showed that both metal/metal and metal/ligand cooperation should be considered for complex cluster systems. Later, N_2O reduction was also observed by a related phosphine-ligated [Cu$_4$S] cluster in the 4Cu^I state,[74] but in that case the mode of N_2O activation has not clearly been elucidated.
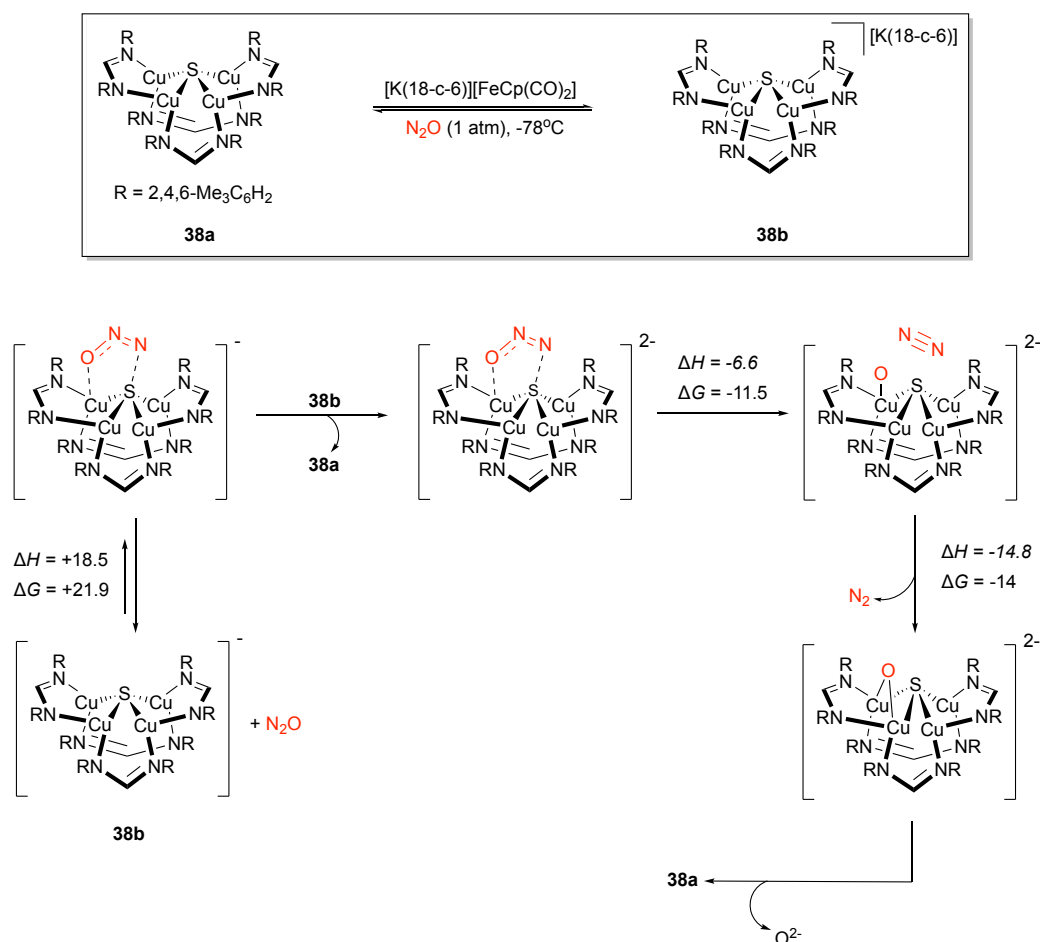
Scheme 38. Synthetic cycle and proposed mechanism for N_2O reduction by a biomimetic Cu$_4$(μ_4-S) cluster.

In 2018, we reported the study of a [Cu$_2$(μ-S)] complex **12a** for its reactivity toward N_2O (as well as CO_2, see Scheme 12).[40] The complex [(IPr*)Cu$_2$(μ-S)] was previously synthesized by Hillhouse and explored for its reactivity towards organic molecules.[39] Here, the [Cu$_2$(μ-S)] complex was exposed to atmospheric N_2O at room temperature (Scheme 28). The primary product from reaction mixtures was [(IPr*)Cu]$_2$(μ-SO$_4$) (**12b**), just as with CO_2. However, unlike CO_2, conducting the N_2O reaction in the presence of PPh$_3$ produced a mixture of **12b** and [(IPr*)Cu]$_2$(μ-O) (**39**) in approximately equimolar ratio. The byproduct Ph$_3$P=S was observed by ^{31}P NMR analysis, indicating the possibility of elemental sulfur elimination. It was proposed that initial oxidation of the [Cu$_2$(μ-S)] complex produces [(IPr*)Cu]$_2$(μ-SO), which either undergoes further oxidation to

form the fully oxidized [(IPr*)Cu]$_2$(μ-SO$_4$) or eliminates elemental sulfur (which is trapped by PPh$_3$) to form [(IPr*)Cu]$_2$(μ-O). In this example, despite the presence of two reduced Cu(I) centers, all the redox chemistry occurs at the bridging sulfur rather than at copper. The [Cu$_2$(μ-S)] motif can be viewed as a model for the dicopper edge of Cu$_Z$ responsible for N_2O activation. Thus, in the absence of additional copper centers bound to the sulfide ligand, the Cu$_Z$ site would be unstable towards sulfide oxidation and/or sulfur-atom extrusion. These observations point to a possible role of the third and fourth Cu centers in Cu$_Z$ beyond mediating electron transfer: protecting the critical Cu-S-Cu unit from irreversible decomposition in the presence of N_2O. Indeed, in the same

ARTICLE

Journal Name

study, trinuclear [(IPr)Cu(μ_3-S)]$^+$ was found to be unreactive towards N$_2$O under the same conditions used for **12a**.
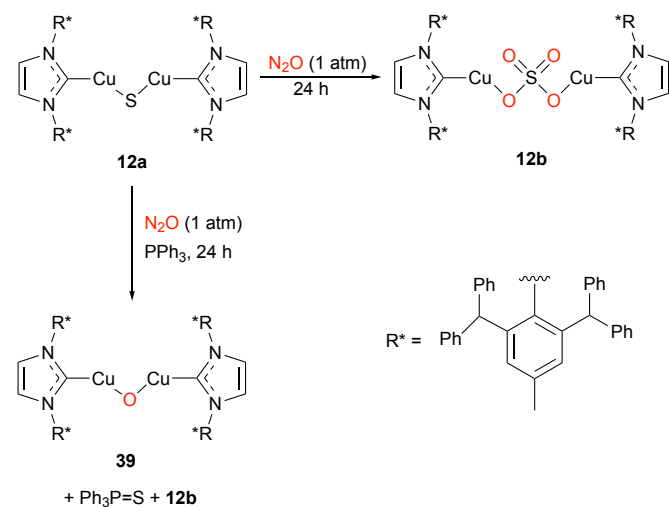
Scheme 39. Reactivity of [Cu$_2$(μ-S)] towards N$_2$O

Other bimetallic complexes

In 2012, Severin and coworkers studied the N$_2$O reactivity of dinuclear ruthenium complexes, (arene)Ru(μ-Cl)$_3$RuCl(C$_2$H$_4$)(PCy$_3$) (arene = *p*-cymene (**40a**) or 1,3,5-C$_6$H$_3$*i*Pr (**40b**) complexes).[75] Exposure of these compounds to N$_2$O (1 atm) produced trinuclear ruthenium products (**40c** or **40d**) (Scheme 40). In addition, an intermediate (**40e** or **40f**) identified by NMR spectroscopy showed an initial loss of ethylene ligand along with O=PCy$_3$ production. This intermediate was shown to react with another N$_2$O equivalent to afford the final, trinuclear product. On the other hand, activation of N$_2$O by a dinuclear ruthenium complex supported by an *N*-heterocyclic carbene (NHC) ligand (**40g**) produced a bimetallic species featuring an oxidized IMes ligand (IMes = 1,3-dimesitylimidazole-2-ylidene) (**40h**) remaining bound to Ru (Scheme 40). NMR and X-ray crystallography data indicated a mixed-valence Ru(II)/Ru(III) assignment for this μ-alkoxide product.
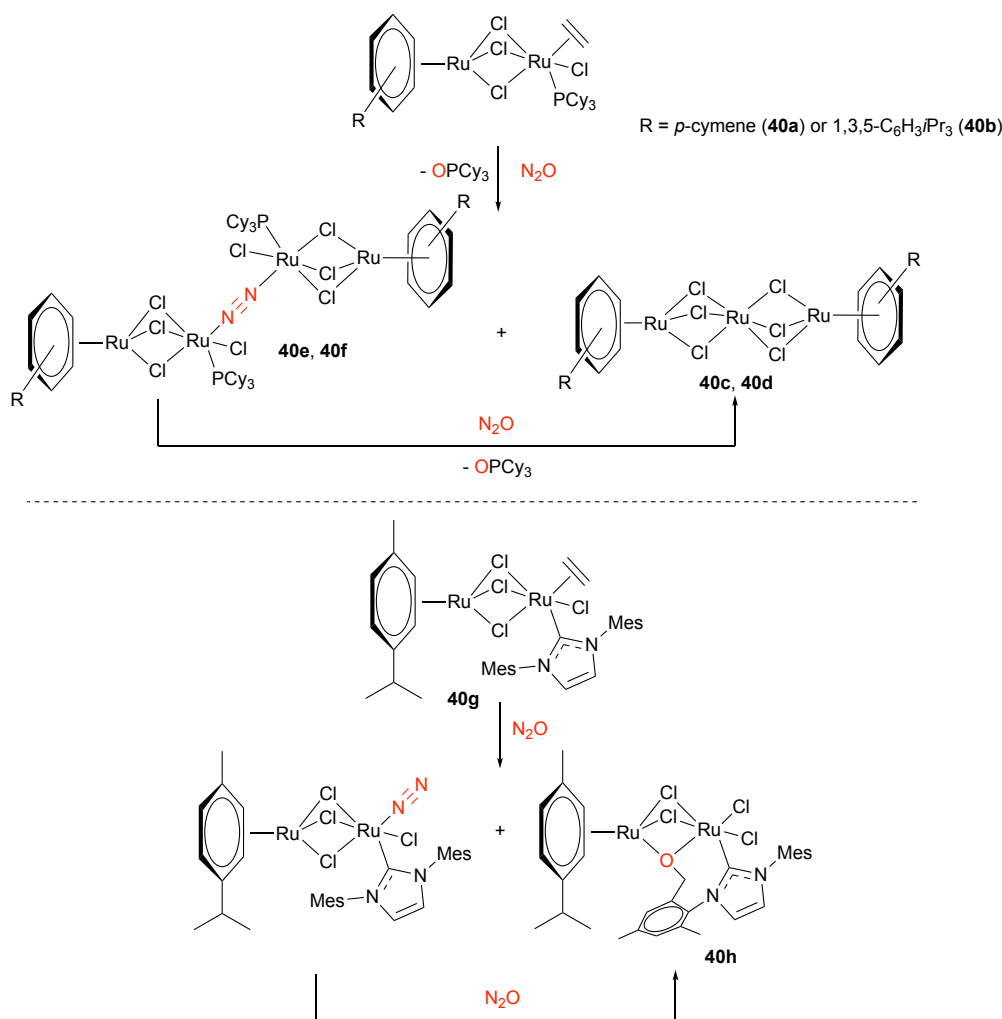
Scheme 40. N$_2$O activation chemistry of diruthenium complexes.

ARTICLE

In 2013, our group reported the syntheses of (IMes)CuFp (**41a**) and (IPr)CuFp (**41b**) (IMes = *N,N'*-bis(2,4,6-trimethylphenyl)imidazole-2-ylidene; IPr = *N,N'*-bis(2,6-diisopropylphenyl)imidazole-2-ylidene; Fp = Fe(Cp)(CO)$_2$).[76] Later, we published the reactivity of these Cu-Fe heterobimetallic complexes and their Cp* analogues, (NHC)CuFp* (Fp* = FeCp*(CO)$_2$), toward N$_2$O.[77] Reaction between (IMes)CuFp and N$_2$O (1 atm) showed an unidentified solid precipitating from the reaction mixtures. According to X-ray energy dispersive spectrum analysis, this insoluble material contained Fe, C, and O as major elemental components. Analysis of headspace above the reaction by GC-MS revealed stoichiometric formation of N$_2$ without evidence of releasing either CO or CO$_2$. However, analysis of the soluble fraction by NMR spectroscopy indicated the formation of (IMes)CuCp (**41c**) (Scheme 41). Similarly, (IPr)CuFp produced (IPr)CuCp (**41d**) after N$_2$O exposure. For the bulkier Cp* derivatives, both Cu-Fe complexes behaved the same way but with much slower reaction rates. Further, the reaction of (IMes)CuFp and N$_2$O in the presence of PPh$_3$ resulted in the formation of OPPh$_3$ (Scheme 30). This product was not observed when PPh$_3$ was added to the reaction mixture after (IMes)CuFp had been exposed to N$_2$O. These observations are consistent with the (NHC)CuFp derivatives reacting with N$_2$O to form a highly reactive, electrophilic oxidizing intermediate that can be intercepted by PPh$_3$ prior to decomposition to (NHC)CuCp and the insoluble solid.

Scheme 41. Reaction of a Cu-Fe heterobinuclear complex with N$_2$O with O-atom transfer to PPh$_3$
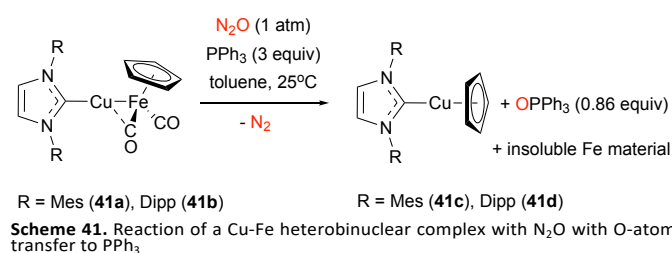
Next, to explore derivatives lacking Cp groups that could migrate from Fe to Cu, in 2020 we reported N$_2$O activation by [(IPr)Cu]$_2$Fe(CO)$_4$ (**42a**) (Scheme 42).[78] Exposure of a **42a** to N$_2$O produced the carbonate complex, [(IPr)Cu]$_2$(μ-CO$_3$) (**42b**), which was characterized crystallographically. An insoluble species also formed in these reactions, which is expected to be 1/n [Fe(CO)$_3$]$_n$ based on reaction stoichiometry. Consistent with this hypothesis, further study of N$_2$O activation in the presence of PPh$_3$ produced *trans*-Fe(CO)$_3$(PPh$_3$)$_2$ (**42c**). In this case, when no Cp group is present, the Fe-bound CO groups apparently become vulnerable to oxidation by N$_2$O.

Scheme 42. N$_2$O reaction by a heterotrinuclear Cu$_2$Fe complex
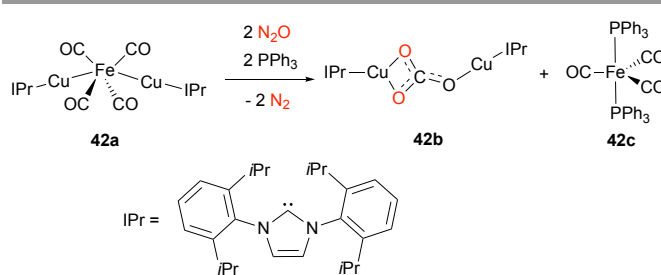
Recently, LaPierre and Maron group reported the activation of N$_2$O using homobimetallic Fe(II) and Co(II) complexes supported by the tris(dialkylamido)-imidophosphorane, NP(pip)$_3$.[79] The reaction between [Fe$_2$(μ_2-NP(pip)$_3$)$_2$(NP(pip)$_3$)$_2$] (**43a**) in diethyl ether and an atmospheric N$_2$O resulted in a μ-oxodiiron complex (**43b**). DFT calculations indicated an initial binding of N$_2$O to one iron center followed by N-O cleavage upon O-coordination to the second iron center (Scheme 43). In this case, the Fe-Fe bond is synergistically reactive toward two-electron reduction of N$_2$O by undergoing one-electron oxidation at each metal center. The related Co(II) derivative showed no reactivity towards N$_2$O under the same condition.

Scheme 43. N$_2$O activation by homobimetallic iron complex #
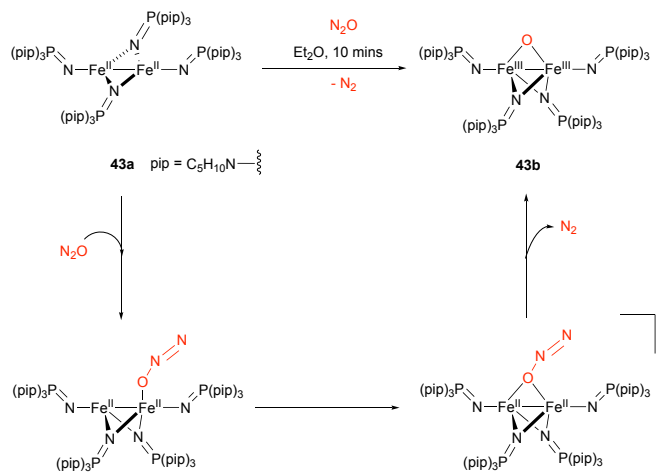
Conclusions

As seen in nature, cooperative bimetallic chemistry is an effective way to activate the kinetically inert molecules, CO$_2$ and N$_2$O. Metals from all over the periodic table are now known to participate in cooperative CO$_2$ activation, including *s*-block, *p*-block, *d*-block, and *f*-block metals and different combinations

thereof. Many examples involve cooperative binding of CO_2 to form metallacarboxylate species, though other identified pathways include reductive disproportionation to CO and CO_3^{2-}, reductive dimerization to $C_2O_4^{2-}$, and oxidative addition to CO and O^{2-}. For N_2O, cooperative bimetallic chemistry is less developed, with most examples involving Cu due to the connection to Cu_Z. Despite the large and growing literature of cooperative bimetallic chemistry for both substrates, it is notable that so few catalytic transformations have emerged.[34,43,53] The difficulty in turning over catalytic cycles derives from the prevailing use of high-energy metal complexes synthesized from alkali metal reduction (or equivalently harsh methods), thus causing the systems to fall into thermodynamic wells with strong M–O bonds installed after CO_2/N_2O activation. A remaining challenge is to develop systems with smaller excess potential built in capable of cooperative bimetallic CO_2/N_2O activation, such that the overall energy landscape for a catalytic process is reasonable to navigate.

Author Contributions

All authors contributed conceptualization, writing, reviewing, and editing of the manuscript.

Conflicts of interest

There are no conflicts to declare.

Acknowledgements

Notes and references

1   J. Hansen and M. Sato, *Proceedings of the National Academy of Sciences*, 2004, **101**, 16109–16114.

2   A. R. Ravishankara, J. S. Daniel and R. W. Portmann, *Science*, 2009, **326**, 123–5.

3   Q. Liu, L. Wu, R. Jackstell and M. Beller, *Nature Communications*, 2015, **6**, 1–15.

4   J. Bao, G. Yang, Y. Yoneyama and N. Tsubaki, *ACS Catalysis*, 2019, **9**, 3026–3053.

5   K. Severin, *Chemical Society Reviews*, 2015, **44**, 6375–6386.

6   J. N. Armor and H. Taube, *Journal of the American Chemical Society*, 1969, **91**, 6874–6876.

7   A. M. Appel, J. E. Bercaw, A. B. Bocarsly, H. Dobbek, D. L. DuBois, M. Dupuis, J. G. Ferry, E. Fujita, R. Hille, P. J. A. Kenis, C. A. Kerfeld, R. H. Morris, C. H. F. Peden, A. R. Portis, S. W. Ragsdale, T. B. Rauchfuss, J. N. H. Reek, L. C. Seefeldt, R. K. Thauer and G. L. Waldrop, *Chemical Reviews*, 2013, **113**, 6621–6658.

8   H. Dobbek, L. Gremer, R. Kiefersauer, R. Huber and O. Meyer, *Proceedings of the National Academy of Sciences of the United States of America*, 2002, **99**, 15971–15976.

9   J.-H. Jeoung and H. Dobbek, *Science*, 2007, **318**, 1461–1464.

10   G. Fachinetti, C. Floriani and P. F. Zanazzi, *Journal of the American Chemical Society*, 1978, **100**, 7405–7407.

11   S. Gambarotta, F. Arena, C. Floriani and P. F. Zanazzi, *Journal of the American Chemical Society*, 1982, **104**, 5082–5092.

12   J. R. Pinkes, B. D. Steffey, J. C. Vites and A. R. Cutler, *Organometallics*, 1994, **13**, 21–23.

13   T. A. Hanna, A. M. Baranger and R. G. Bergman, *Journal of the American Chemical Society*, 1995, **117**, 11363–11364.

14   L. H. Gade, *Angewandte Chemie-International Edition in English*, 2000, **39**, 2658–2678.

15   C. M. Mömming, E. Otten, G. Kehr, R. Fröhlich, S. Grimme, D. W. Stephan and G. Erker, *Angewandte Chemie - International Edition*, 2009, **48**, 6643–6646.

16   E. M. Johnston, C. Carreira, S. Dell'Acqua, S. G. Dey, S. R. Pauleta, I. Moura and E. I. Solomon, *Journal of the American Chemical Society*, 2017, **139**, 4462–4476.

17   I. Bar-Nahum, A. K. Gupta, S. M. Huber, M. Z. Ertem, C. J. Cramer and W. B. Tolman, *Journal of the American Chemical Society*, 2009, **131**, 2812–2814.

18   E. Otten, R. C. Neu and D. W. Stephan, *Journal of the American Chemical Society*, 2009, **131**, 9918–9919.

19   J. S. Woertink, P. J. Smeets, M. H. Groothaert, M. A. Vance, B. F. Sels, R. A. Schoonheydt and E. I. Solomon, *Proceedings of the National Academy of Sciences of the United States of America*, 2009, **106**, 18908–18913.

20   M.-L. L. Tsai, R. G. Hadt, P. Vanelderen, B. F. Sels, R. A. Schoonheydt and E. I. Solomon, *Journal of the American Chemical Society*, 2014, **136**, 3522–3529.

21   D. Gau, R. Rodriguez, T. Kato, N. Saffon-Merceron, A. de Cózar, F. P. Cossío and A. Baceiredo, *Angewandte Chemie International Edition*, 2011, **50**, 1092–1096.

22   X. Chen, H. Wang, S. Du, M. Driess and Z. Mo, *Angewandte Chemie International Edition*, 2022, **61**, e202114598.

23   T. Ouyang, H.-J. Wang, H.-H. Huang, J.-W. Wang, S. Guo, W.-J. Liu, D.-C. Zhong and T.-B. Lu, *Angewandte Chemie International Edition*, 2018, **57**, 16480–16485.

24   Z. Guo, G. Chen, C. Cometto, B. Ma, H. Zhao, T. Groizard, L. Chen, H. Fan, W.-L. Man, S.-M. Yiu, K.-C. Lau, T.-C. Lau and M. Robert, *Nature Catalysis*, 2019, **2**, 801–808.

25   M. Cheng, Y. Yu, X. Zhou, Y. Luo and M. Wang, *ACS Catalysis*, 2019, **9**, 768–774.

26   M. E. Ahmed, S. Adam, D. Saha, J. Fize, V. Artero, A. Dey and C. Duboc, *ACS Energy Letters*, 2020, **5**, 3837–3842.

27   H. Chen, L. Chen, G. Chen, M. Robert and T. C. Lau, *ChemPhysChem*, 2021, **22**, 1835–1843.

28   A. F. R. Kilpatrick and F. G. N. Cloke, *Chemical Communications*, 2014, **50**, 2769–2771.

29   A. F. R. Kilpatrick, J. C. Green and F. G. N. Cloke, *Organometallics*, 2015, **34**, 4816–4829.

30   A. Noor, S. Qayyum, T. Bauer, S. Schwarz, B. Weber and R. Kempe, *Chemical Communications*, 2014, **50**, 13127–13130.

31   A. Paparo, J. S. Silvia, C. E. Kefalidis, T. P. Spaniol, L. Maron, J. Okuda and C. C. Cummins, *Angewandte Chemie*

International Edition, 2015, **54**, 9115–9119.

32   J. P. Krogman, B. M. Foxman and C. M. Thomas, *Journal of the American Chemical Society*, 2011, **133**, 14582–14585.

33   J. P. Krogman, M. W. Bezpalko, B. M. Foxman and C. M. Thomas, *Inorganic Chemistry*, 2013, **52**, 3022–3031.

34   R. Angamuthu, P. Byers, M. Lutz, A. L. Spek and E. Bouwman, *Science*, 2010, **327**, 313–315.

35   C. T. Saouma, M. W. Day and J. C. Peters, *Chemical Science*, 2013, **4**, 4042–4051.

36   R. Shimogawa, T. Takao, G. I. Konishi and H. Suzuki, *Organometallics*, 2014, **33**, 5066–5069.

37   C. M. Palit, D. J. Graham, C. H. Chen, B. M. Foxman and O. V. Ozerov, *Chemical Communications*, 2014, **50**, 12840–12842.

38   H. Wu, J. Li, D. Yang, P. Tong, J. Zhao, B. Wang and J. Qu, *Inorganic Chemistry Frontiers*, 2019, **6**, 2185–2193.

39   J. Zhai, A. S. Filatov, G. L. Hillhouse and M. D. Hopkins, *Chem Sci*, 2016, **7**, 589–595.

40   S. Bagherzadeh and N. P. Mankad, *Chemical Communications*, 2018, **54**, 1097–1100.

41   J. R. Prat, C. A. Gaggioli, R. C. Cammarota, E. Bill, L. Gagliardi and C. C. Lu, *Inorganic Chemistry*, 2020, **59**, 14251–14262.

42   M. Devillard, R. Declercq, E. Nicolas, A. W. Ehlers, J. Backs, N. Saffon-Merceron, G. Bouhadir, J. C. Slootweg, W. Uhl and D. Bourissou, *Journal of the American Chemical Society*, 2016, **138**, 4917–4926.

43   R. C. Cammarota, M. V. Vollmer, J. Xie, J. Ye, J. C. Linehan, S. A. Burgess, A. M. Appel, L. Gagliardi and C. C. Lu, *Journal of the American Chemical Society*, 2017, **139**, 14244–14250.

44   J. Hicks, A. Mansikkamäki, P. Vasko, J. M. Goicoechea and S. Aldridge, *Nature Chemistry*, 2019, **11**, 237–241.

45   D. Sorbelli, L. Belpassi and P. Belanzoni, *Journal of the American Chemical Society*, 2021, **143**, 14433–14437.

46   C. McManus, J. Hicks, X. Cui, L. Zhao, G. Frenking, J. M. Goicoechea and S. Aldridge, *Chemical Science*, 2021, **12**, 13458–13468.

47   H. Liu, R. J. Schwamm, M. S. Hill, M. F. Mahon, C. L. McMullin and N. A. Rajabi, *Angewandte Chemie International Edition*, 2021, **60**, 14390–14393.

48   L. Escomel, I. Del Rosal, L. Maron, E. Jeanneau, L. Veyre, C. Thieuleux and C. Camp, *Journal of the American Chemical Society*, 2021, **143**, 4844–4856.

49   S. Sinhababu, M. Radzhabov and N. P. Mankad, *ChemRxiv*, , DOI:10.33774/chemrxiv-2021-xt242.

50   R. Lalrempuia, A. Stasch, A. Stasch and C. Jones, *Chemical Science*, 2013, **4**, 4383–4388.

51   M. D. Anker, M. Arrowsmith, P. Bellham, M. S. Hill, G. Kociok-Köhn, D. J. Liptrot, M. F. Mahon and C. Weetman, *Chemical Science*, 2014, **5**, 2826–2830.

52   A. J. Boutland, I. Pernik, A. Stasch and C. Jones, *Chemistry – A European Journal*, 2015, **21**, 15749–15758.

53   C. Weetman, P. Bag, T. Szilvási, C. Jandl and S. Inoue, *Angewandte Chemie*, 2019, **131**, 11077–11081.

54   C. Weetman, A. Porzelt, P. Bag, F. Hanusch and S. Inoue, *Chemical Science*, 2020, **11**, 4817–4827.

55   O. P. Lam, S. C. Bart, H. Kameo, F. W. Heinemann and K. Meyer, *Chemical Communications*, 2010, **46**, 3137–3139.

56   L. Castro, O. P. Lam, S. C. Bart, K. Meyer and L. Maron, *Organometallics*, 2010, **29**, 5504–5510.

57   A. Schmidt, F. W. Heinemann, C. E. Kefalidis, L. Maron, P. W. Roesky and K. Meyer, *Chemistry – A European Journal*, 2014, **20**, 13501–13506.

58   A.-C. Schmidt, A. V. Nizovtsev, A. Scheurer, F. W. Heinemann and K. Meyer, *Chemical Communications*, 2012, **48**, 8634.

59   D. H. Woen, G. P. Chen, J. W. Ziller, T. J. Boyle, F. Furche and W. J. Evans, *Angewandte Chemie - International Edition*, 2017, **56**, 2050–2053.

60   V. Mougel, C. Camp, J. Pécaut, C. Copéret, L. Maron, C. E. Kefalidis and M. Mazzanti, *Angewandte Chemie International Edition*, 2012, **51**, 12280–12284.

61   O. Cooper, C. Camp, J. Pécaut, C. E. Kefalidis, L. Maron, S. Gambarelli and M. Mazzanti, *Journal of the American Chemical Society*, 2014, **136**, 6716–6723.

62   L. Castro, S. Labouille, D. R. Kindra, J. W. Ziller, F. Nief, W. J. Evans and L. Maron, *Chemistry - A European Journal*, 2012, **18**, 7886–7895.

63   M. Xémard, V. Goudy, A. Braun, M. Tricoire, M. Cordier, L. Ricard, L. Castro, E. Louyriac, C. E. Kefalidis, C. Clavaguéra, L. Maron and G. Nocton, *Organometallics*, 2017, **36**, 4660–4668.

64   A. Formanuik, F. Ortu, C. J. Inman, A. Kerridge, L. Castro, L. Maron and D. P. Mills, *Chemistry - A European Journal*, 2016, **22**, 17976–17979.

65   C. J. Inman, A. S. P. Frey, A. F. R. Kilpatrick, F. G. N. Cloke and S. M. Roe, *Organometallics*, 2017, **36**, 4539–4545.

66   A. R. Willauer, D. Toniolo, F. Fadaei-Tirani, Y. Yang, M. Laurent and M. Mazzanti, *Dalton Transactions*, 2019, **48**, 6100–6110.

67   S. C. Rathnayaka and N. P. Mankad, *Coordination Chemistry Reviews*, 2021, **429**, 213718.

68   P. Chen, S. I. Gorelsky, S. Ghosh and E. I. Solomon, *Angewandte Chemie International Edition*, 2004, **43**, 4132–4140.

69   W. B. Tolman, *Angewandte Chemie International Edition*, 2010, **49**, 1018–1024.

70   C. Esmieu, M. Orio, S. Torelli, L. Le Pape, J. Pécaut, C. Lebrun and S. Ménage, *Chem. Sci.*, 2014, **5**, 4774–4784.

71   B. J. Johnson, W. E. Antholine, S. V. Lindeman and N. P. Mankad, *Chem Commun*, 2015, **51**, 11860–11863.

72   B. J. Johnson, W. E. Antholine, S. V. Lindeman, M. J. Graham and N. P. Mankad, *Journal of the American Chemical Society*, 2016, **138**, 13107–13110.

73   S. C. Rathnayaka, C. W. Hsu, B. J. Johnson, S. J. Iniguez and N. P. Mankad, *Inorganic Chemistry*, 2020, **59**, 6496–6507.

74   C.-W. W. Hsu, S. C. Rathnayaka, S. M. Islam, S. N. MacMillan and N. P. Mankad, *Angewandte Chemie - International Edition*, 2020, **59**, 627–631.

75   A. G. Tskhovrebov, E. Solari, R. Scopelliti and K. Severin, *Organometallics*, 2012, **31**, 7235–7240.

76   U. Jayarathne, T. J. Mazzacano, S. Bagherzadeh and N. P. Mankad, *Organometallics*, 2013, **32**, 3986–3992.

77   U. Jayarathne, S. R. Parmelee and N. P. Mankad, *Inorganic chemistry*, 2014, **53**, 7730–7737.

78   Y. Lakliang and N. P. Mankad, *Organometallics*, 2020, **39**, 2043–2046.

79   L. M. Aguirre Quintana, Y. Yang, A. Ramanathan, N. Jiang, J. Bacsa, L. Maron and H. S. La Pierre, *Chemical Communications*, 2021, **57**, 6664–6667.